



DIPLOMA THESIS

Spread Spectrum Positioning Accuracy in Noisy Multipath Environments

performed at the

Institute of Electrical Measurements and Circuit Design
at the Vienna University of Technology

supervised by

Univ.Ass. Dipl.-Ing. Dr.techn. Holger Arthaber

and

o.Univ.Prof Dipl.-Ing. Dr.techn. Gottfried Magerl

Martin Lerch
9825204
Frankgasse 13
3400 Klosterneuburg

Vienna, November 2008



DIPLOMARBEIT

Spread Spectrum Positioning Accuracy in Noisy Multipath Environments

Ausgeführt zum Zwecke der Erlangung des akademischen Grades eines Diplom-Ingenieurs
unter der Leitung von

Univ.Ass. Dipl.-Ing. Dr.techn. Holger Arthaber

und

o.Univ.Prof Dipl.-Ing. Dr.techn. Gottfried Magerl

am

Institut für Elektrische Mess- und Schaltungstechnik

eingereicht an der Technischen Universität Wien
Fakultät für Elektrotechnik und Informationstechnik

von

Martin Lerch
9825204
Frankgasse 13
3400 Klosterneuburg

Wien, November 2008

Abstract

Positioning and ranging systems working with the propagation delay from different sources in order to derive the current position, often make use of direct spread spectrum modulation techniques. In this thesis, the impact of noise, multipath propagation, and pulse shaping at the transmitter onto the ranging accuracy of such systems is investigated.

For the purpose of comparing different pulse shapes regarding their robustness against noise and multipath propagation, a MATLAB simulation system was set up. This system simulates the influence of white gaussian noise and multipath propagation onto bandlimited rectangular and root raised cosine shaped signals. The simulation for white gaussian noise showed that root raised cosine pulses perform better than rectangular pulses. In the next step this behaviour of the system was analytically proved by deriving the Cramer Rao lower bound for the impact of white gaussian noise onto both kinds of pulses. The analytical result followed the simulation outcome. The simulation run including multipath propagation showed too an additional accuracy for the root raised cosine pulses.

A hardware testbed was set up for the purpose of measuring the influence of noise and other interferers. In this system, which is fully controlled by MATLAB, arbitrary signals of up to 21 MHz bandwidth can be transmitted and the propagation time can be estimated with an accuracy equal to a ranging error of approximately 1 mm. The noise floor of the receiver was used to compare the simulated and calculated results with the measurements in the testbed.

Kurzfassung

Positioning Systeme, die Signallaufzeit von unterschiedlichen Stationen dazu benutzen die Position eines Objekts zu bestimmen benutzen hauptsächlich Spread Spectrum Modulation. Diese Diplomarbeit beschäftigt sich mit den Auswirkungen von Rauschen, Mehrwegeausbreitung und den verwendeten Pulsformen auf die Genauigkeit der Laufzeitmessung solcher Systeme.

Um die einzelnen Pulse bezüglich ihrer Robustheit gegenüber Rauschen und Mehrwegeausbreitung vergleichen zu können, wurde eine MATLAB Simulationsumgebung geschaffen. Mit diesem System wurde der Einfluss von weißem gausschen Rauschen und Mehrwegeausbreitung auf Signale mit Root raised cosine und bandlimitierter Rechteck Filterung simuliert. Das Ergebnis der Simulation für weißes gaussches Rauschen war ein deutlich geringerer Fehler bei der Verwendung von Root raised cosine Pulsen als bei Rechteckpulsen. Weiters wurde mittels der Cramer Rao lower bound der Einfluss von weissem gausschen Rauschen für beide Pulstypen hergeleitet. Die Berechnungen untermauerten die Ergebnisse der Simulation. Die Simulation für Mehrwegeausbreitung zeigte ebenfalls einen geringeren Fehler bei der Verwendung von Root raised cosine Pulsen.

Weiters wurde ein Messsystem zur Bestimmung des Einflusses von Rauschen und anderer Störer aufgebaut. Mit diesem komplett von MATLAB gesteuerten System lassen sich Laufzeiten von beliebigen Signalen mit Bandbreiten bis zu 21 MHz mit einer Genauigkeit von umgerechnet ca. 1 mm messen. Das Empfängerrauschen wurde dazu benutzt die Ergebnisse der Simulation und der Berechnung für weisses gaussches Rauschen denen der Messungen gegenüberzustellen.

Contents

1	Introduction	1
1.1	Radio positioning	1
1.1.1	Time of arrival	2
1.1.2	Time difference of arrival	2
1.2	Direct sequence spread spectrum modulation	4
1.2.1	The matched filter approach	6
1.2.2	Spread spectrum in positioning	7
2	Implementation	8
2.1	Spreading sequences	9
2.1.1	Maximum length sequences	9
2.1.2	Gold codes	10
2.2	Pulses	12
2.2.1	Bandlimited rectangular pulses	12
2.2.2	Root raised cosine pulses	13
2.3	Implementation in MATLAB	16
3	White gaussian noise	19
3.1	The AWGN channel	19
3.2	Simulation	20
3.3	The Cramer Rao lower bound	21
3.3.1	Bandlimited rectangular pulses	21
3.3.2	Root raised cosine pulses	24
3.4	Discussion	26
3.4.1	The observation time	27
4	Multipath propagation	29
4.1	Ranging errors due to multipath propagation	29
4.2	Simulation	30
4.2.1	Rectangular pulses	31
4.2.2	Root raised cosine pulses	32
4.2.3	Comparison	32
5	The measurement system	34
5.1	Transmitter	35
5.1.1	The AMIQ signal generator	35
5.1.2	The SMIQ vector modulator	38
5.2	Receiver	38
5.2.1	The 70 MHz IF sampler	38
5.2.2	Equalization	41
5.3	Synchronization	42

6	Measurements	45
6.1	Aspects	45
6.2	White gaussian noise	46
7	Conclusion	48
	Bibliography	50
A	The Demonstration GUI	51

List of Figures

1.1	Locating a transmitter or receiver	1
1.2	Spherical positioning in time of arrival systems	2
1.3	Hyperbolic positioning in time difference of arrival systems	3
1.4	Spread spectrum system with a correlator receiver	4
1.5	Signals in a spread spectrum system with a correlator receiver	5
1.6	Matched filter spread spectrum system	6
1.7	Parallel correlators as matched filter receiver	6
1.8	Signals in a matched filter spread spectrum system	7
2.1	The matched filter spread spectrum system	8
2.2	Generation of m sequences using a shift register	10
2.3	Generation of Gold sequences by adding two m sequences	10
2.4	Autocorrelation of m sequences and Gold sequences	11
2.5	Crosscorrelation of m sequences and Gold sequences	11
2.6	Rectangular pulses for a fixed chiprate	13
2.7	Rectangular pulses with a fixed bandwidth	13
2.8	Raised cosine pulses as Nyquist pulses	14
2.9	Raised cosine pulses with a fixed bandwidth	15
2.10	Positioning error due to sampling	16
3.1	The AWGN channel	19
3.2	Simulation of the influence of white noise	20
3.3	Approximation for rectangular pulses	23
3.4	Standard deviation for root raised cosine pulses	26
3.5	Comparison of rectangular and root raised cosine pulses	27
4.1	Multipath propagation	29
4.2	Ranging errors due to multipath propagation	30
4.3	Simulation in the baseband	30
4.4	Multipath error as a function of the phase	31
4.5	Multipath error for rectangular pulses	31
4.6	Multipath error for root raised cosine pulses	32
4.7	Multipath errors in comparison of different pulses	32
5.1	Measurement system	34
5.2	Transmitter	35
5.3	Sinc distortion at the DAC output	36
5.4	Receiver	38
5.5	Passband to baseband transformation	39
5.6	Sampler input characteristic	41
5.7	Known and unknown trigger delay	42
5.8	Comparison of free run and 10 MHz synchronization	42

5.9	Synchronization of the sample clocks	43
5.10	Configurations	44
6.1	Mean error as a function of the SNR	46
6.2	Influence of the equalizer for $\alpha = 0$	47
6.3	Influence of the equalizer for $\alpha = 1$	47
A.1	Demonstration GUI	52
A.2	Demodulated data	52
A.3	Channel distortion	53
A.4	Histogram	53

Chapter 1

Introduction

1.1 Radio positioning

Radio positioning, radio navigation or radio locating is the process of finding the location of objects through the use of radio waves. *Radio locating* usually denotes passive systems, where the radio waves are transmitted by the object to be located or backscattered, as in radar. In active systems, the location is determined by the object itself.

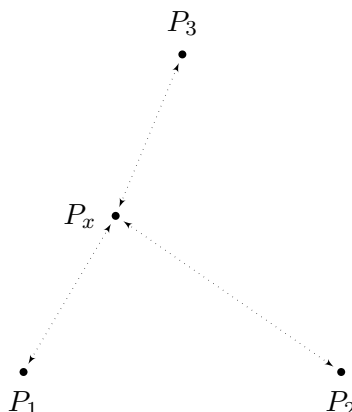


Figure 1.1: Locating a transmitter/receiver using a system of receivers/transmitters at known positions.

Figure 1.1 shows a system with a reference network consisting of antennas at known positions $P_1 - P_3$ and an antenna at the position P_x that shall be determined. Depending on the application, at P_x may be a transmitter and the position P_x is determined by the reference network or a receiver at P_x calculates its position using the signals that are transmitted by the reference antennas at $P_1 - P_3$.

For a configuration of antennas as in Figure 1.1, there are two major techniques that use propagation times of signals for the determination of a position:

- **Time of arrival (TOA):** The distances from the transmitter(s) to the receiver(s) are determined by measuring the propagation times.
- **Time difference of arrival (TDOA):** The difference of the distances is determined by measuring the differences of the propagation times from the transmitters(s) to the receiver(s).

1.1.1 Time of arrival

The position of an object is calculated using the distances from the object to reference points, whereas the distances are calculated by measuring the propagation time of a signal from the transmitter to the receiver. The objects position is then given by the intersection of spheres (in the three dimensional space) or by the intersection of circles (on a two dimensional plane). For a unique determination of a position, four distances are needed (three on a two dimensional plane).

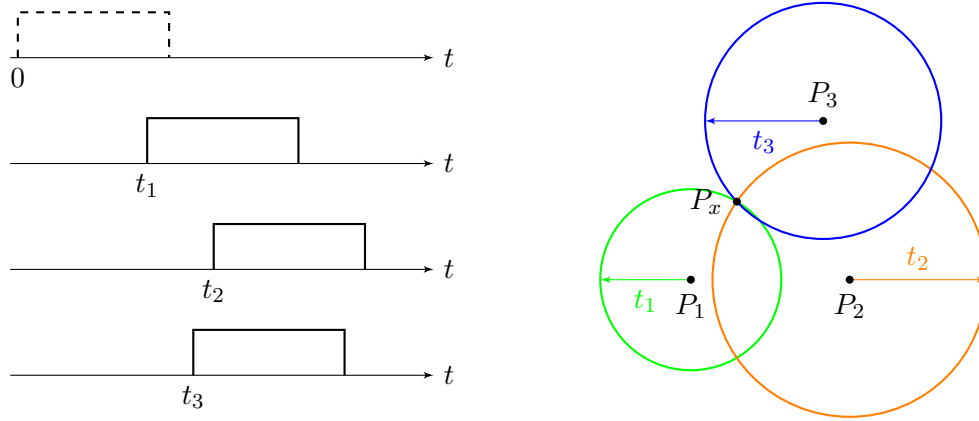


Figure 1.2: Spherical positioning in time of arrival systems.

Figure 1.2 illustrates the *spherical positioning* using the distances to three different reference points. Whereas it does not make a difference in which direction the propagation time is measured. A device at P_x may be a receiver for the signals transmitted by the reference stations, or it may be a transmitter and the reference network measures the distances to the unknown position P_x .

In order to measure the propagation time of a signal, receivers and the transmitters have to be synchronized. The common way of synchronization in TOA systems is to use synchronous clocks in all transmitters and receivers.

1.1.2 Time difference of arrival

In TDOA systems, time differences between the arrival of signals are used to determine a position. The common application of TDOA systems is to determine the position of a transmitter using a system of several receivers at known positions. As in TOA, TDOA may also be used the other way round, where a receiver calculates its position by measuring the time difference of arrival of the signals from reference transmitters.

Figure 1.3 illustrates the calculation of a position using TDOA. The calculated position is given by the intersection of hyperbolas (in 2D) or hyperboloids (in 3D). On these hyperbolas (or hyperboloids), the difference of the distances from the unknown position to two reference positions is constant. The number of receivers (or transmitters) needed for a unique solution is the same as for TOA, three for two dimensions and four for three dimensions. In most

applications it is sufficient to use just three receivers (or transmitters). One of the two resulting positions can then usually be excluded.

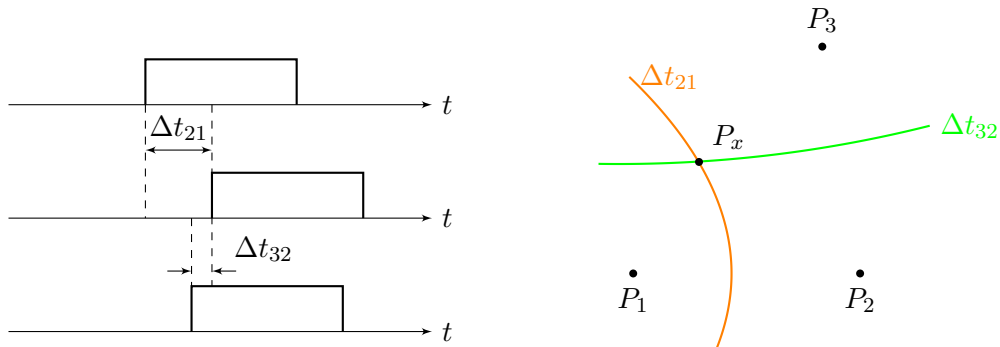


Figure 1.3: Hyperbolic positioning in time difference of arrival systems.

Synchronization

Depending on whether a transmitter or a receiver is at the position to determine, different kinds of synchronizations are needed:

- If the position of a transmitter is calculated in the reference system, the measurement of the times the signal arrives at the different antennas has to be done synchronously.
- If the position is calculated in a receiver at the unknown position, the transmit signals have to be send synchronously as well as the measurement in the receiver has to be done synchronously.

1.2 Direct sequence spread spectrum modulation

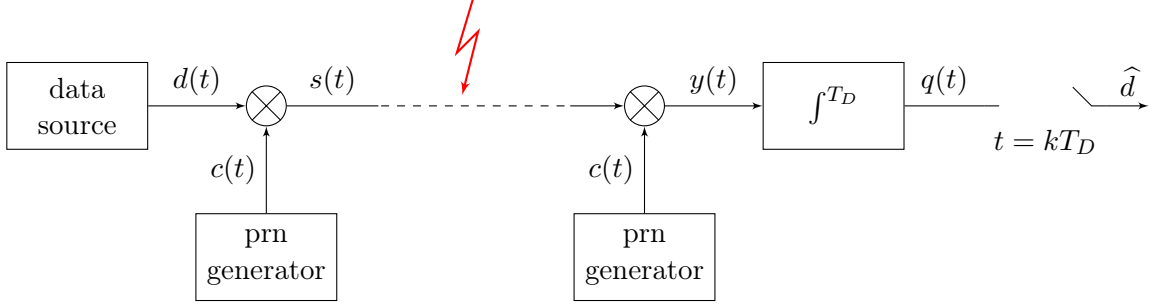


Figure 1.4: Spread spectrum system with a correlator receiver.

Direct sequence spread spectrum is a digital modulation technique that takes much more transmit bandwidth than the information signal that is being modulated. The data symbols are multiplied by a continuous sequence of chips, each of which has a much shorter duration than a data symbol, resulting in a noise like transmit signal having the symbol energy spread over a very large bandwidth. Because of this property, the spreading sequences are also called *pseudorandom noise* or *pseudo noise*. In the receiver the correlation of the received signal with a local copy of the spreading sequence is calculated. Therefore, the used spreading sequence has to be known by the receiver.

The common criterion to compare the quality of direct sequence spread spectrum systems is the process gain:

$$G_p = \frac{\text{SNR}_{out}}{\text{SNR}_{in}} \quad (1.1)$$

where SNR_{out} is the signal-to-noise ratio after the demodulation and SNR_{in} is the signal-to-noise ratio at the input of the receiver. For direct sequences spread spectrum, G_p equals the ratio between the chiprate and the symbolrate, or equivalently the length L of the spreading sequence in number of chips. For typical process gains of 10 to 30 dB, the system may also work for negative signal-to-noise ratios at the input of the receiver and may tolerate jamming power levels higher than the received signal power. Thus, direct sequence spread spectrum modulation can be used for secure communication, where the transmit signal can be hid in noise and the received signal can only be demodulated if the used spreading sequence is known.

Direct sequence spread spectrum modulation can be used for CDMA¹ applications, where several transmitters, that use different spreading sequences share the same channel, limited by the cross-correlation properties of the spreading sequences (see Section 2.1).

Figure 1.5 illustrates a typical direct sequence spread spectrum transmission using a system like the one in Figure 1.4:

- In the transmitter, the data symbols $d(t)$ are multiplied by the periodic spreading sequence $c(t)$, resulting in a transmit bandwidth that equals the bandwidth of the spread-

¹Code division multiple access

ing sequence. For a spreading sequence of length L , the transmit bandwidth is L times the bandwidth of the unmodulated data (the chiprate is L times the symbolrate).

- The received signal $s(t)$ is multiplied by the same spreading sequence that was used in the modulator. Assuming synchronization between the receiver and the transmitter, the result of the multiplication is the original data signal with the data bandwidth.
- Uncorrelated interferers, like the CW² signal $i(t)$ in Figure 1.5 are spread spectrum modulated by the receiver, the interferers energy is spread over the bandwidth of the spreading sequence.
- The integrator calculates the sum of the despread signal $y(t)$ over one symbol period, whereas the output of the integrator $q(t)$ at $t = k \cdot T_D$ is the autocorrelation of the spreading sequence at $\tau = 0$. For broadband noise, like spreaded interferers, the integrator acts as a lowpass filter.
- In order to obtain the data symbols $d[kT_D]$, the signal at the output of the integrator is sampled at the symbol rate.

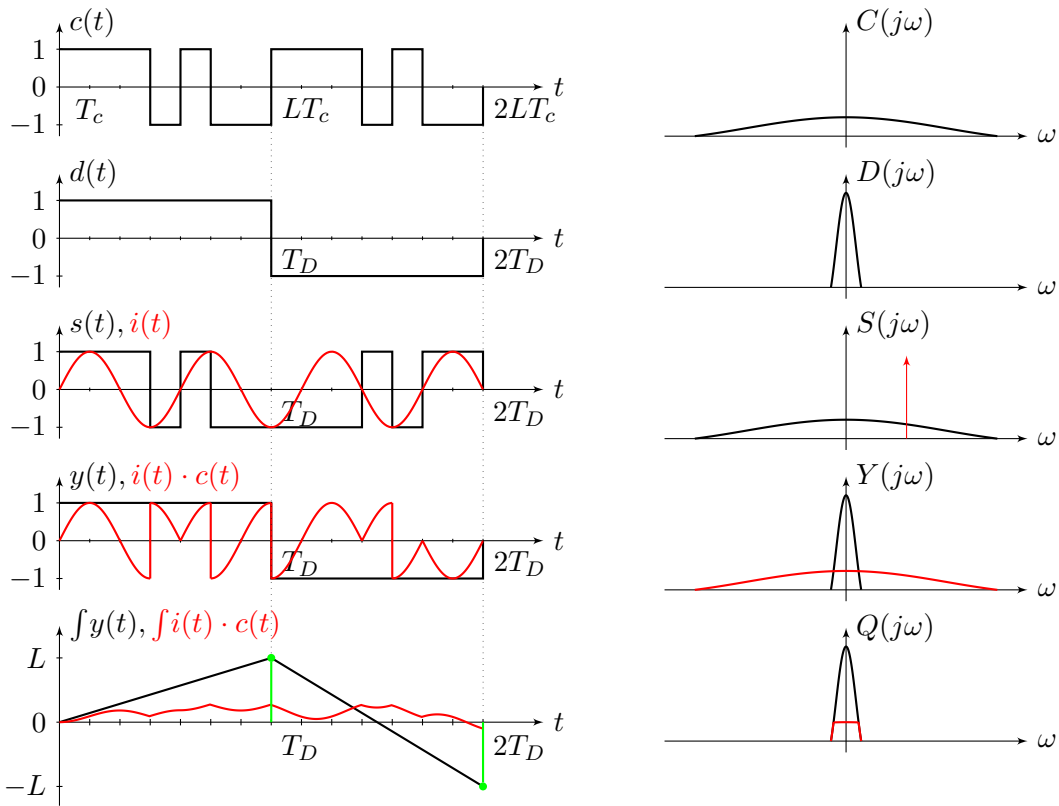


Figure 1.5: Signals in a spread spectrum system with a correlator receiver.

²continuous wave

1.2.1 The matched filter approach

In telecommunications, a linear receive filter is called matched filter if its impulse response is the time-reversed of the transmit filters impulse response. The output of the receive filter is the auto-correlation of the transmit pulse and it can be shown that then the signal-to-noise ratio after the receive filter is maximized. Such a matched filter can be used to demodulate a direct sequence spread spectrum signal.

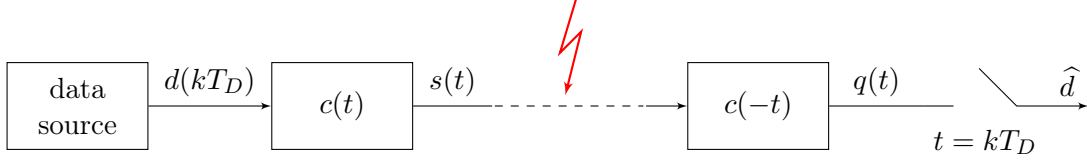


Figure 1.6: Matched filter spread spectrum system.

Figure 1.6 shows a spread spectrum system which uses a linear filter for modulation and the corresponding matched filter for demodulation. While the transmit signal is exactly the same as for the correlator system described before, the output of the demodulator is the complete correlation function for all time differences τ :

$$q(\tau) = \int_0^{T_D} s(t)c(t - \tau) dt \quad (1.2)$$

Figure 1.8 shows the signals in a matched filter system. For $t = k \cdot T_D$, the output of the matched filter equals the output of the correlator receiver. Figure 1.7 illustrates the differences between these two approaches. While a single correlator calculates the correlation for a single code phase, the matched filter calculates the correlation function for all values of the codephase.

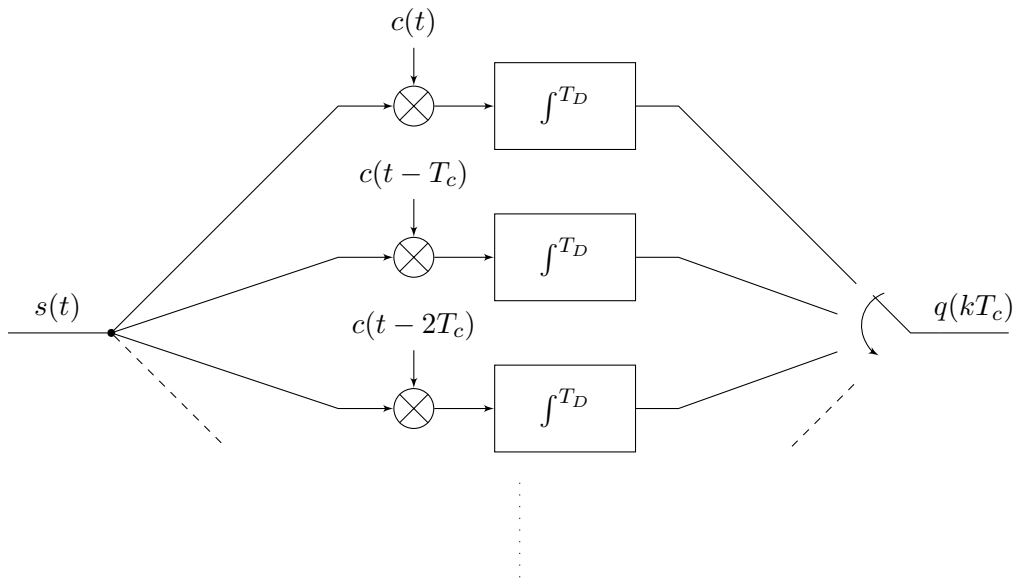


Figure 1.7: Parallel correlators as matched filter receiver.

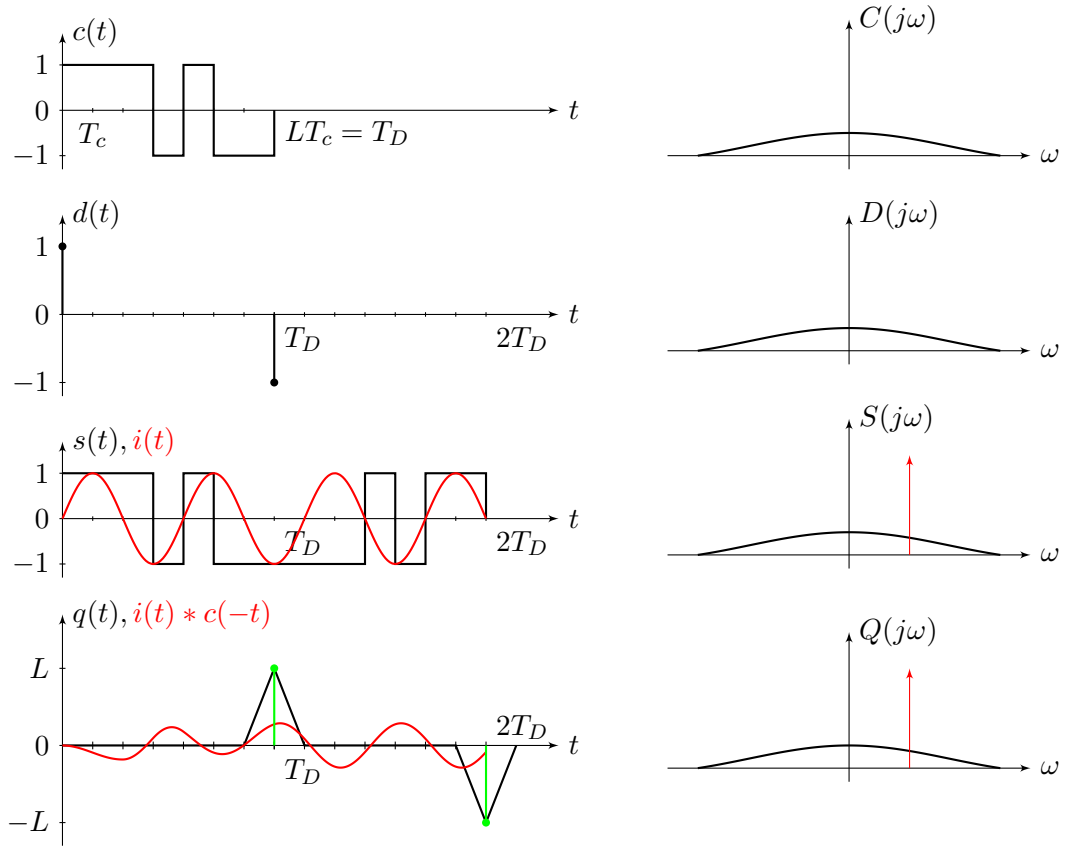


Figure 1.8: Signals in a matched filter spread spectrum system.

1.2.2 Spread spectrum in positioning

For both techniques of radio positioning described in Chapter 1.1, the time of the arrival of a signal is measured in the receiver. Using direct sequence spread spectrum modulation, the estimation of the time a signal arrives equals the process of synchronizing the receiver to the received signal. This is done by maximizing the correlation function of the received signal $c_r(t)$ with the local reference signal $c_{ref}(t)$:

$$\hat{\tau} = \arg \max_{\tau} \int_0^T c_r(t) c_{ref}(t - \tau) dt \quad (1.3)$$

whereas:

- in correlator receivers, the synchronization is a search for the correlation maximum by shifting the codephase of the local copy of the spreading sequence until the maximum is found.
- in matched filter receivers, the correlation function is calculated for all values of the code phase in one step. Thus the synchronization equals the search for the maximum of the output signal $q(t)$ before the symbol rate sampler.

Chapter 2

Implementation

In this chapter, a simulation system for direct sequence spread spectrum modulation using matched filters is introduced and the design and implementation in MATLAB is described.

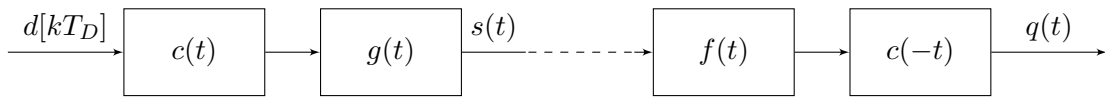


Figure 2.1: The matched filter spread spectrum system.

In the design of the system, the following aspects were considered:

- **Receiver:** For the simulation, as well as for the measurement system in Chapter 5, a matched filter receiver was used. A very simple way to implement a matched filter receiver is described in the last section.
- **Spreading sequences:** Two different types of spreading sequences were implemented:
 - m-sequences, with their very good autocorrelation properties.
 - gold codes, for use in CDMA systems.
- **Filters:** For the transmit filter, that limits the transmit bandwidth to a certain value and the receive filter, that filters out all of the out-of-band interferers and noise, matched filters were used. Whereas root raised cosine and bandlimited rectangular pulses were implemented.

Figure 2.1 shows an overview of the used system, that consists of four filters, the spread spectrum modulation and demodulation matched filters $c(t)$ and $c(-t)$, and the matched transmit and receive filters $g(t)$ and $f(t) = g(-t)$.

2.1 Spreading sequences

In spread spectrum receivers the correlation of the received sequence with the local copy of the spreading sequence is calculated. Thus, the correlation function is used as criterion for the comparison of different spreading sequences or families of spreading sequences [1].

- In order to compare single sequences, the periodic¹ autocorrelation function of the sequences $c_n(t)$ is calculated.

$$acf(\tau) = \int_{t=0}^{T_D} c_n(t)c_n(t+\tau) dt \quad 0 \leq \tau \leq T_D \quad (2.1)$$

The criteria for a good autocorrelation function are:

- A high maximum of $acf(\tau)$ at $\tau = 0$.
 - A low number of maxima for $\tau \neq 0$.
 - Low maxima for $\tau \neq 0$.
- For the comparison of different families of spreading sequences concerning their qualities in CDMA applications, the crosscorrelation between different sequences of the same family is calculated.

$$ccf(\tau) = \int_{t=0}^{T_D} c_n(t)c_m(t+\tau) dt \quad 0 \leq \tau \leq T_D \quad (2.2)$$

The crosscorrelation function of an ideal family of sequences is zero (the sequences are orthogonal). For common families of spreading sequences, the value of the maximum of the crosscorrelation function is used as criterion.

2.1.1 Maximum length sequences

Maximum length sequences (m-sequences) are having a nearly perfect autocorrelation function and so they are often used in direct sequence spread spectrum systems. Their autocorrelation function takes only two values:

$$acf[k] = \begin{cases} L & k = 0 \\ -1 & 1 \leq k \leq L-1 \end{cases} \quad (2.3)$$

The maximum of the autocorrelation function equals the length L of one period and the only maximum for $k \neq 0$ is -1 .

¹The begin of the sequence is connected to its end resulting in a ring

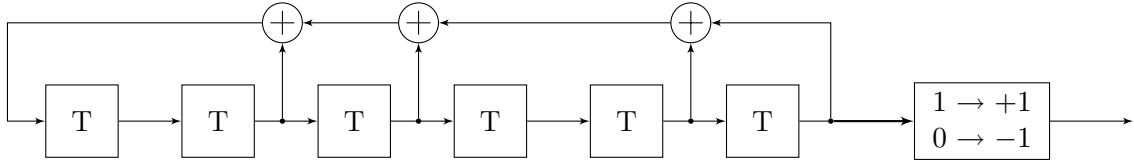


Figure 2.2: Generation of m sequences using a shift register.

Figure 2.2 shows the common way to generate m-sequences using a linear feedback shift register where the input on the left is fed by the XOR sum calculated over certain bits of the current internal state. The linear feedback shift register cycles through all possible binary words (with exception of the zero word), whereas the initial word may be any binary number except the zero word. The result is a periodic sequence of maximum length $L = 2^n - 1$, with n being the length of the shift register. The number of "1"s is one greater than the number of "0"s, thus, after the mapper the sequence is approximately zero-mean resulting in a carrier suppression.

For the use in CDMA systems, different sequences of the same length are needed. The different sequences are then generated by shift registers having different feedback taps, whereas not all possible feedback configurations generate sequences of maximum length (See Table 2.1 for the number of different m-sequences with a certain length). The values, the crosscorrelation function takes depends on which specific pair of m-sequences was used. Figure 2.5 (a) shows a typical crosscorrelation function of m-sequences.

2.1.2 Gold codes

Gold codes (Gold sequences) are very popular spreading sequences in CDMA applications. They are generated by adding two different m-sequences of the same length, whereas not all pairs of m-sequences result in Gold codes. Those pairs which yield Gold codes are called *preferred pairs*. The length of the resulting Gold code is the same as of the used m-sequences ($L=2^n - 1$).

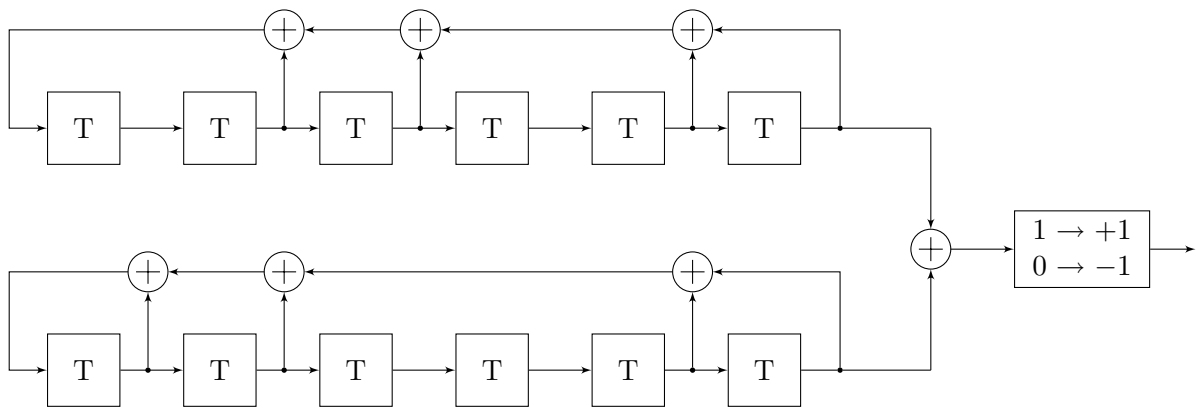


Figure 2.3: Generation of Gold sequences by adding two m sequences.

The generation of Gold codes is illustrated in Figure 2.3. For a fixed initial value of the first m-sequence, every different initial value of the second m-sequence results in a different Gold code. One set of Gold codes consists of the preferred pair of m-sequences plus all Gold codes

that can be generated by adding these two sequences. Thus, the number of gold codes in one set is $L + 2 = 2^n + 1$. The crosscorrelation function takes the same three values for any two Gold codes in the same set (see Figure 2.5 (b)).

The autocorrelation functions of m and gold sequences are shown in Figure 2.4. While maximum length sequences have nearly perfect autocorrelation properties, the autocorrelation of gold sequences has significant maxima for $\tau \neq 0$.

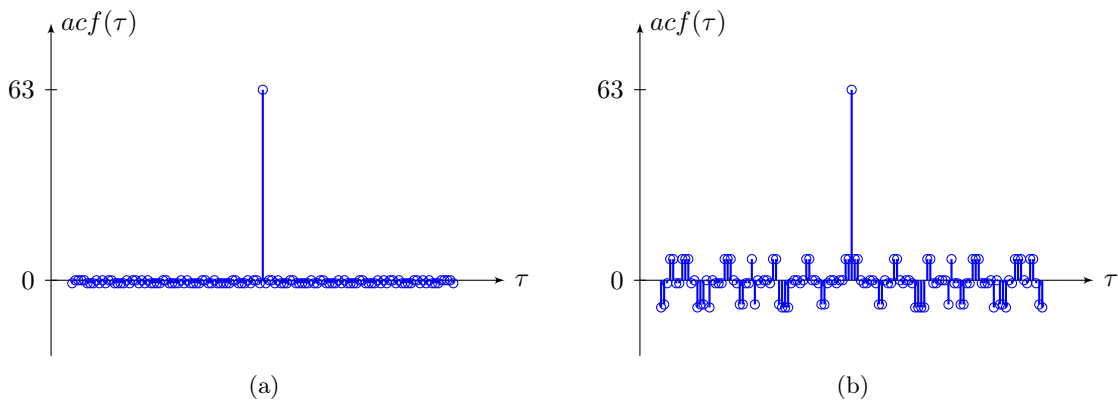


Figure 2.4: Autocorrelation of (a) m sequences and (b) Gold sequences.

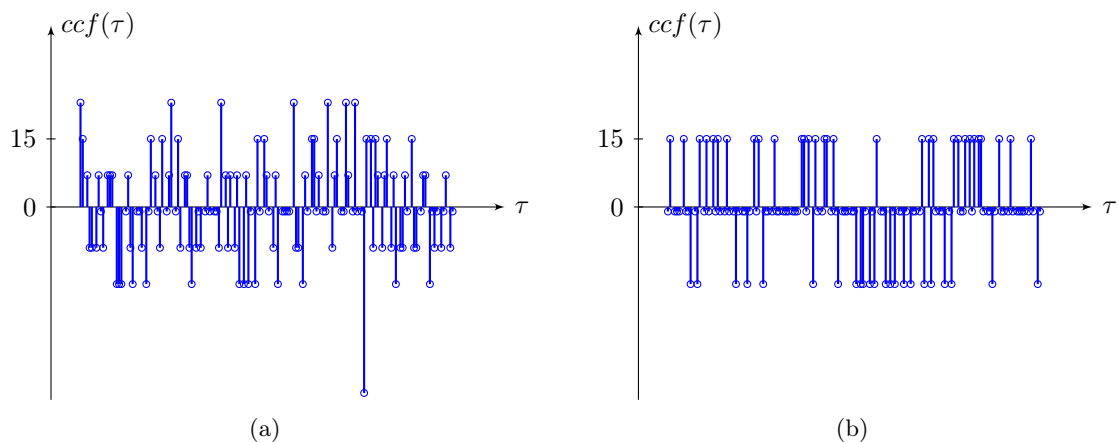


Figure 2.5: Crosscorrelation of (a) m sequences and (b) Gold sequences.

A comparison of both types of sequences is given by Table 2.1. The number of available sequences for a certain sequence length is for Gold sequences much higher than for m-sequences. The maximum value of the crosscorrelation function is much lower for Gold sequences as for m sequences. The longer the sequences, the higher the differences between the two types of sequences.

		m sequences		Gold sequences	
SR length	seq. length	seq. in set	max. CCF	seq. in set	max CCF
3	7	2	5	9	3
4	15	2	9	17	7
5	31	6	11	33	7
6	63	6	23	65	15
7	127	18	41	129	15
8	255	16	95	257	31
9	511	48	113	513	31
10	1023	60	383	1025	63
11	2047	176	287	2049	63
12	4095	144	1407	4097	127

Table 2.1: Comparison of m and Gold - sequences.

2.2 Pulses

The shape of the output pulse of the spread spectrum system is given by the transmit and the receive filter. For a matched filter system, where the impulse response of the receive filter is the time inverted impulse response of the transmit filter, the overall pulse $p(t)$ is the autocorrelation of the impulse response of the transmit filter. In the following, the two different types of pulses that were used are explained.

2.2.1 Bandlimited rectangular pulses

Ideal rectangular pulses, without any limitation of the bandwidth, have an infinite transmit bandwidth. The Fourier transform for a chiprate R_c is given by Eq. (2.4).

$$S(j\omega) = 2 \frac{\sin(\frac{\omega}{2R_c})}{\omega} \quad (2.4)$$

The autocorrelation is the triangular function:

$$p(t) = \begin{cases} 1 - \left| \frac{t}{T_c} \right| & |t| \leq T_c \\ 0 & |t| > T_c \end{cases} \quad (2.5)$$

For the use in radio communication, where the transmit bandwidth is limited, rectangular pulses have to be low pass filtered before they can be used. Figure 2.6 (a) shows the autocorrelation of rectangular pulses that were filtered using an ideal lowpass filter. The smaller the transmit bandwidth, the more the lowpass filter becomes evident. For a given chiprate, the shape of the pulse is determined by the bandlimitation.

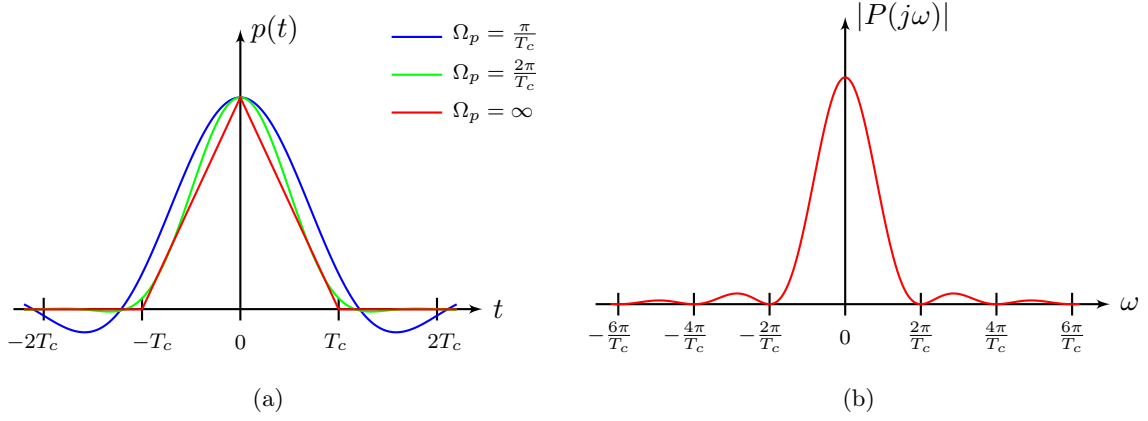


Figure 2.6: Rectangular pulses for a fixed chiprate and different bandwidths:
(a) Autocorrelation and (b) Fourier transform for an infinite bandwidth.

Figure 2.7 shows a comparison of bandlimited rectangular pulses for a given bandwidth and different values of the chiprate. The width of the pulse is given by the chiprate, the lower the chiprate, the more the resulting pulse looks like the ideal rectangular pulse and the higher the width of the pulse.

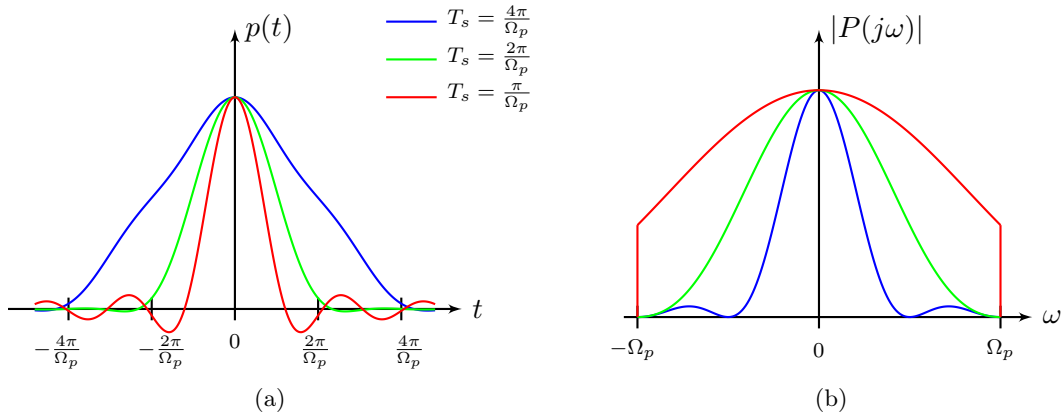


Figure 2.7: Rectangular pulses with a fixed bandwidth and different chiprates:
(a) Autocorrelation and (b) Fourier transform.

2.2.2 Root raised cosine pulses

Root raised cosine pulses [2] are very popular transmit pulses in telecommunications. In a system that uses root raised cosine pulses in the transmitter and receiver (matched filters), the overall pulse is a so called raised cosine pulse. If a raised cosine filtered signal is sampled correctly in the receiver, no intersymbol interference occurs and the data symbols are perfectly recovered. Pulses with this property are called Nyquist pulses.

The impulse response of the raised cosine pulse (that equals the autocorrelation of the root raised cosine pulse) is given by:

$$p(t) = \omega_\alpha(t) \cdot \text{sinc}\left(\pi \frac{t}{T_c}\right) \quad \text{with} \quad \omega_\alpha(t) = \frac{\cos\left(\alpha \pi \frac{t}{T_c}\right)}{1 - \left(2\alpha \frac{t}{T_c}\right)^2} \quad (2.6)$$

with the roll-off factor $\alpha \in [0, 1]$. The Fourier transform is given by

$$P(j\omega) = \begin{cases} T_c & |\omega| \leq (1 - \alpha) \frac{\pi}{T_c} \\ \frac{T_c}{2} \left[1 - \sin\left(\frac{T_c}{2\alpha} \left(|\omega| - \frac{\pi}{T_c}\right)\right) \right] & (1 - \alpha) \frac{\pi}{T_c} \leq |\omega| \leq (1 + \alpha) \frac{\pi}{T_c} \\ 0 & |\omega| \geq (1 + \alpha) \frac{\pi}{T_c} \end{cases} \quad (2.7)$$

This shows that raised cosine pulses are bandlimited with bandwidth

$$\Omega_p = (1 + \alpha) \frac{\pi}{T_c} \quad (2.8)$$

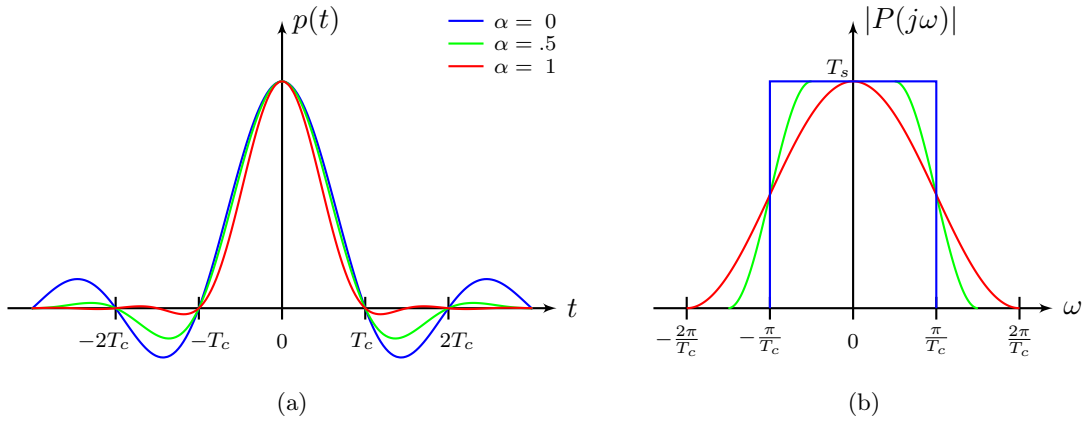


Figure 2.8: Raised cosine pulses as nyquist pulses: (a) Time-domain function, (b) Fourier transform.

Figure 2.8 shows the autocorrelation and the Fourier transform of raised cosine pulses for three different values of the roll-off factor α . A larger roll-off factor means slower spectral roll-off, larger bandwidth and better temporal concentration of the pulse. For $\alpha = 0$, the raised cosine pulse degenerates to the sinc pulse².

Figure 2.9 shows raised cosine pulses for a given bandwidth Ω_p . The impulse response and the Fourier transform can be derived by substituting the chip duration by:

$$T_c = (1 + \alpha) \frac{\pi}{\Omega_p} \quad (2.9)$$

² $p(t) = \text{sinc}\left(\pi \frac{t}{T_c}\right)$

This implementation of raised cosine pulses will be used in Chapter 3, where the influence of noise is derived as a function of the bandwidth. Compared to the common implementation of raised cosine pulses, the width of the pulse is the higher, the higher the roll-off factor.

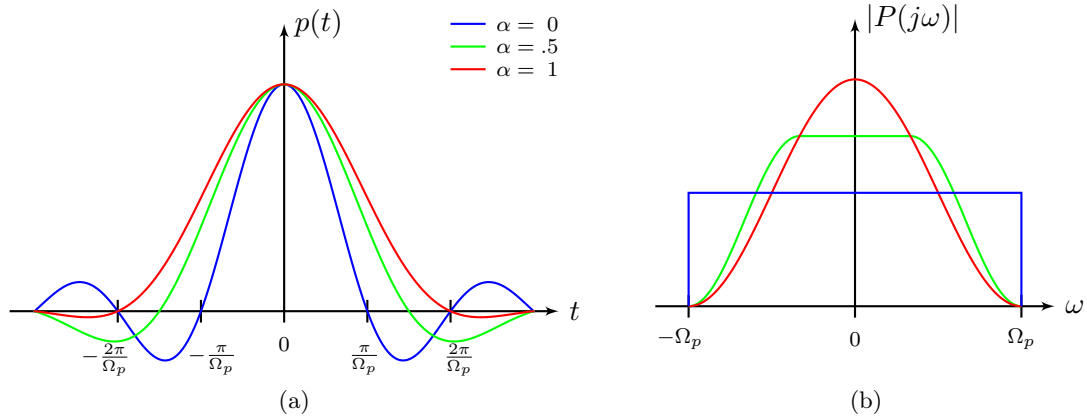


Figure 2.9: Raised cosine pulses with a fixed bandwidth: (a) Time-domain function, (b) Fourier transform.

2.3 Implementation in MATLAB

In order to simulate the influence of white noise and multipath propagation, a simulation system was implemented in MATLAB. The same system was also used in the measurement system in Chapter 5.

The most important aspects are described in the following:

The sample rate

The simulation in MATLAB is done using discrete-time signals. Therefore a system sample rate has to be chosen. Simulations showed that for typical signals errors caused by white noise and multipath channels are much smaller than the length of one chip, so the sample rate has to be much higher than the chiprate and much higher than the signal bandwidth. Figure 2.10 illustrates the limited positioning resolution of discrete-time signals. For equally likely distributed positions, the mean error for a sample rate of $f_s = 1/T_s$ is:

$$\sigma_\tau^2 = \int_{-\frac{T_s}{2}}^{\frac{T_s}{2}} t^2 \frac{1}{T_s} dt = \frac{T_s^2}{12} \quad (2.10)$$

$$\sigma_\tau = \frac{T_s}{\sqrt{12}} \quad (2.11)$$

In order to measure other errors, the error due to the discrete-time simulation should be smaller than the error that shall be measured. Thus, the sampling rate has to be sufficiently high.

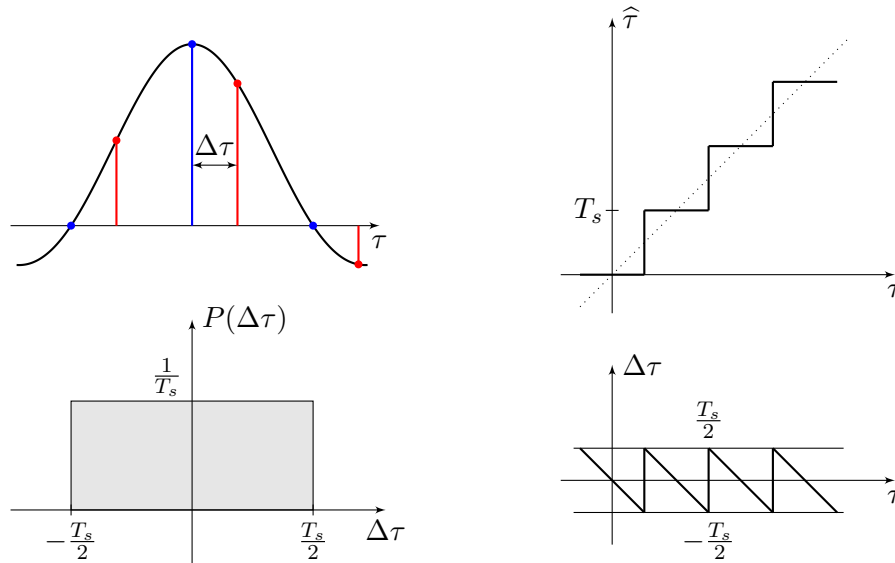


Figure 2.10: Positioning error due to sampling.

Using the resample function

Instead of using extremely high system sample rates, MATLAB's *resample*³ function may be used. The signals are then generated and transmitted at lower sample rates. In the receiver, the received signal, or equivalently the output of the modulator is resampled to a higher sample rate. Simulations showed that the sample rate in the transmitter should be at least four times the signal bandwidth. Otherwise, the distortion due to the reconstruction filter of the resample function becomes evident.

Signal generation in the frequency domain

For the simulation of the estimation of the propagation time, a periodic transmit signal was used, whereas its sufficient to generate, transmit, and process a single period.

- The spreading sequences are generated in MATLAB functions, whereas the length of the shift register can be chosen from 2 to 12. In typical simulations, the sample rate is higher than the chiprate. Thus, the sequence has to be upsampled using MATLAB's *upsample*⁴ function. Whereas the sample rate has to be an integer multiple of the chiprate.
- The root raised cosine filters were implemented in a function that calculates the impulse response for arbitrary values of the sample rate, the bandwidth, and the roll-off factor. The same function is used for the bandlimitation of rectangular pulses where a root raised cosine filter with $\alpha = 0$ is used.
- The transmit signal is the spreading sequence filtered by the transmit filter, whereas the filtering is done in the frequency domain using the FFT⁵. One period of the spreading sequence as well as the impulse response of the transmit filter is FFT transformed, whereas the length of the FFT is for both signals the period of the spreading sequence. The multiplication of both equals the cyclic convolution. The resulting signal, transformed back to the time domain, is one period of the periodic spreading sequence filtered by the transmit filter.
- The same technique can be used when the transmit signal shall be modulated with data. The spreading sequence is first modulated with the data symbols, and is then filtered in the frequency domain.

Signal processing in the frequency domain

Like the transmitter, the receiver can also be implemented in the frequency domain. The receiver consist of two linear filters which are both the time inverted versions of one of the filters in the transmitter. Thus, one period of the transmit signal can be used to demodulate the received signal. The received signal is transformed to the frequency domain and multiplied by the complex conjugate of the FFT transform of the transmit signal. Transformed back to the time domain, the result is one period of the output of the matched filter receiver for a periodic receive signal.

³The resample function inserts zeros between the samples and filters the resulting signal with a reconstruction filter.

⁴The upsample function inserts zeros between the samples, but does not filter the resulting signal.

⁵Fast Fourier Transformation

The final simulation system

The following code illustrates the generation and processing of direct sequence spread spectrum signals in MATLAB.

```
pn_n=10;    % Length of the shift register
fc=10;      % Chiprate
fs=1000;    % System sample rate
fg=5;       % Signal bandwidth
a=1;        % Roll off factor
d=50;       % Length of the impulse response of the filters
```

After defining the signal parameters, the spreading sequence and the transmit filter are generated and transformed to the frequency domain using the FFT.

```
prn_seq=mfolgen(pn_n,1,1,1);           % Spreading sequence
prn_seq=upsample(prn_seq,fs/fc);        % Upsampling
PRN=fft(prn_seq,length(prn_seq));       % FFT

cos_filter=raisedcosine(fs,fg,a,d);     % Calculation of the filter
RRC=fft(cos_filter.numr,length(prn_seq)); % FFT
```

One period of the transmit signal is calculated in the frequency domain

```
s=ifft(PRN.*RRC);    % Transmit signal
```

and the receive filter is the conjugate complex of the Fourier transform of the transmit signal.

```
REC=conj(PRN.*RRC);  % The (matched) receive filter
```

The received signal y is filtered and demodulated by calculating the correlation.

```
q=ifft(fft(y).*REC); % Demodulation
```

Finally, the delay of the received signal is estimated by finding the maximum of the demodulated signal.

```
[m i]=max(q);        % m...maximum, i...position of the maximum
```

Chapter 3

White gaussian noise

In this chapter, the influence of white gaussian noise on the estimation of the signal position will be inspected. The influence is simulated and a lower bound is derived. In the last section, the influence of the signal parameters and the role of the observation time will be discussed.

3.1 The AWGN channel

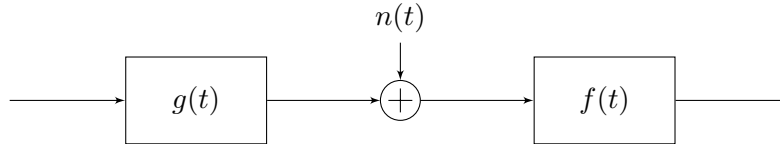


Figure 3.1: The AWGN channel.

An AWGN (Additive white Gaussian noise) channel adds zero-mean noise with a constant spectral density and a gaussian distribution of amplitude to the transmitted signal. Whereas the noise is at least white inside the used frequency band. White noise with a gaussian distribution may have many different natural sources, like the thermal vibrations of atoms. For this thermal noise, the one-sided noise PSD¹ is $N_0 = k\vartheta$, where k is the Boltzmann's constant ($1.380 \cdot 10^{-23} \text{ J/K}$) and ϑ is the temperature in Kelvin. The total noise power of white noise within a certain bandwidth B is $N_0 B$.

In order to compare different transmit signals regarding the influence of white noise, it is useful to use the concept of the signal-to-noise ratio. In this work, two different definitions of the signal-to-noise ratio were used:

- $\text{SNR} = \frac{\text{signal power}}{\text{noise power}}$
- $\frac{C}{N_0} = \frac{\text{symbol energy}}{\text{one-sided noise PSD}}$

While the first definition is a rather general definition, the second one is usually used in telecommunications. To substitute one definition by the other, Eq. (3.1) can be used:

$$\frac{C}{N_0} = \text{SNR} \cdot B \cdot T_D \quad (3.1)$$

where T_D is the symbol duration.

¹Power spectral density

3.2 Simulation

In order to see the influence of white gaussian noise on the estimated position $\hat{\tau}$ of the correlation maximum, noise with a certain power was added to the transmit signal and the position of the maximum of the correlation function was determined. This was repeated N times and the standard deviation (Eq. (3.2)) over these N results was calculated.

$$\sigma_{\tau} = \sqrt{\frac{1}{N-1} \sum_{i=1}^N (\hat{\tau}_i - \bar{\tau})^2} \quad (3.2)$$

The following aspects had to be considered in the simulation:

- The mean error for quite large values of the signal-to-noise ratio is much smaller than the width of the received pulse. In order to achieve a resolution higher than the errors, a sample rate much higher than the signal bandwidth has to be used.
- Simulations showed that the sample duration should be at least four times smaller than the expected error to obtain useful results.
- The generation of the noise was done by MATLAB's *randn* function, which generates a sequence of zero-mean random values with a gaussian distribution.
- Simulations showed that the standard deviation should be calculated over at least 500 results for every value of the signal-to-noise ratio to obtain useful results.

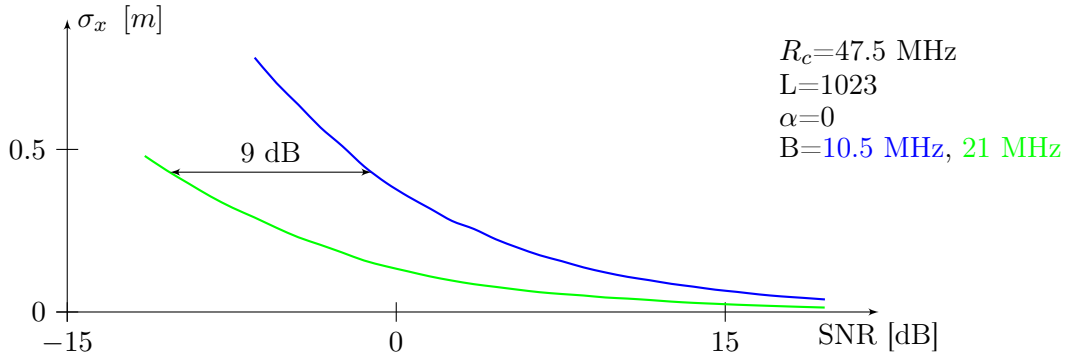


Figure 3.2: Simulation of the influence of white noise.

Figure 3.2 shows the result of a simulation using root raised cosine pulses with two different transmit bandwidths. Independent of the shape of the pulse, the error is indirectly proportional to the square-root of the signal-to-noise ratio. The characteristic for a certain signal is just shifted to the left or the right when a signal parameter is changed.

As in Figure 3.2, the error characteristic is shifted to the left by 9 dB when the bandwidth is doubled, or in other words, for a certain error, the SNR is up to 9 dB lower for a signal having twice the bandwidth.

The minimum signal-to-noise ratio

While the estimated positions for strong signals are located mostly within the pulsewidth (the correlation maximum is much higher than the standard deviation of the noise), the higher the noise power gets, the more noise peaks are higher than the correlation maximum and the estimated positions become equally likely distributed over the whole signal period. In the simulation, this becomes evident by an abrupt rise of the mean error. In Figure 3.2, the mean error is only plotted for values of the SNR greater than this minimum SNR. The simulations showed that this minimum SNR is reduced by $\approx 3\text{dB}$ when the bandwidth is doubled.

3.3 The Cramer Rao lower bound

Even though the simulation of the influence of white noise works quite fine, a lower bound for the mean error was derived using the Cramer Rao lower bound, that expresses a lower bound on the variance of estimators of a deterministic parameter.

For the used estimator:

$$\hat{\tau} = \arg \max_{\tau} \int_0^T c_r(t) c_{ref}(t - \tau) dt \quad (3.3)$$

a way to calculate the Cramer Rao lower bound was found in [3]:

$$\sigma_{\tau}^2 \geq \frac{1}{8\pi^2 \left(\frac{C}{N_0} \right) \left[\frac{\int_{-B}^B f^2 |S_m(f)|^2 df}{\int_{-B}^B |S_m(f)|^2 df} \right]} \quad (3.4)$$

Where $S_m(f)$ is the Fourier transform of the transmit waveform.

In the following, this lower bound is calculated for bandlimited rectangular pulses and for root raised cosine pulses.

3.3.1 Bandlimited rectangular pulses

For unfiltered rectangular pulses, the Fourier transform is:

$$S_m(f) = \frac{R_c}{\pi} \frac{\sin(\frac{\pi f}{R_c})}{f} \quad (3.5)$$

Since the two integrals are calculated in the frequency domain, the bandlimitation is done by the limits of the integrals.

With $\phi = 2\pi \frac{f}{R_c}$, $\frac{d\phi}{df} = \frac{2\pi}{R_c}$, and $\Phi = 2\pi \frac{B}{R_c}$, the solutions of the two integrals are:

$$\begin{aligned}
\int_{-B}^B f^2 |S_m(f)|^2 df &= \frac{R_c^2}{\pi^2} \int_{-B}^B \sin^2\left(\frac{\pi f}{R_c}\right) df = \frac{R_c^3}{2\pi^3} \int_{-\Phi}^{\Phi} \sin^2\left(\frac{\phi}{2}\right) d\phi = \frac{R_c^3}{2\pi^3} \left(\frac{\phi}{2} - \frac{1}{2} \sin(\phi)\right) \Big|_{-\Phi}^{\Phi} \\
&= \frac{R_c^3}{2\pi^3} (\Phi - \sin(\Phi)) = \frac{R_c^2}{\pi^2} \left(B - \frac{R_c}{2\pi} \sin\left(\frac{2\pi B}{R_c}\right)\right)
\end{aligned} \tag{3.6}$$

$$\begin{aligned}
\int_{-B}^B |S_m(f)|^2 df &= \frac{2R_c}{\pi} \int_{-\Phi}^{\Phi} \frac{\sin^2(\frac{\phi}{2})}{\phi^2} dx = \frac{R_c}{\pi} \int_{-\Phi}^{\Phi} \frac{1}{\phi^2} - \frac{\cos(\phi)}{\phi^2} dx = \frac{R_c}{\pi} \left(\frac{\cos(\phi) - 1}{\phi} + \text{Si}(\phi)\right) \Big|_{-\Phi}^{\Phi} \\
&= \frac{2R_c}{\pi} \left(\frac{\cos(\Phi) - 1}{\Phi} + \text{Si}(\Phi)\right) = \frac{R_c}{\pi} \left(\frac{R_c \cos(\frac{2\pi B}{R_c}) - 1}{B} + 2\text{Si}\left(\frac{2\pi B}{R_c}\right)\right)
\end{aligned} \tag{3.7}$$

$$\begin{aligned}
\frac{\int_{-B}^B f^2 |S_m(f)|^2 df}{\int_{-B}^B |S_m(f)|^2 df} &= \frac{\frac{R_c^3}{2\pi^3} (\Phi - \sin(\Phi))}{\frac{2R_c}{\pi} \left(\frac{\cos(\Phi) - 1}{\Phi} + \text{Si}(\Phi)\right)} = \frac{\frac{\Phi R_c^2}{4\pi^2} (\Phi - \sin(\Phi))}{(\cos(\Phi) - 1 + \Phi \text{Si}(\Phi))} \\
&= \frac{BR_c}{2\pi} \frac{(\Phi - \sin(\Phi))}{(\cos(\Phi) - 1 + \Phi \text{Si}(\Phi))}
\end{aligned} \tag{3.8}$$

The Cramer Rao lower bound for bandlimited rectangular pulses finally is²:

$$\sigma_\tau \geq \sqrt{\frac{\cos(\Phi) - 1 + \Phi \text{Si}(\Phi)}{4\pi \frac{C}{N_0} BR_c (\Phi - \sin(\Phi))}} \quad \text{with} \quad \Phi = 2\pi \frac{B}{R_c} \tag{3.9}$$

Approximations

In order to compare the lower bound for rectangular pulses to the lower bound for root raised cosine pulses, approximations for the exact solution in (3.9) should be used.

For integer values of the ratio of the bandwidth B to the chiprate R_c , the lower bound is:

$$\sigma_{\tau,n} = \sqrt{\frac{\text{Si}(2\pi n)}{4\pi \frac{C}{N_0} BR_c}} \quad \text{for} \quad n = \frac{B}{R_c} = 1, 2, \dots \tag{3.10}$$

² $\text{Si}(x) = \int_0^x \frac{\sin(\xi)}{\xi} d\xi$

or equivalently, with the values listed in Figure 3.3 (b):

$$\sigma_{\tau,n} = \frac{b}{\sqrt{\frac{C}{N_0} B R_c}} \quad \text{with} \quad b = \sqrt{\frac{\text{Si}(2\pi \frac{B}{R_c})}{4\pi}} \quad (3.11)$$

Considering a given chiprate, the approximation is always a lower bound for bandwidths higher than the bandwidth used in the approximation (see the plot of the Si function in Figure 3.3 (a)).

For very large values of $\frac{B}{R_c}$, the following approximation can be used:

$$\sigma_{\tau,\infty} = \frac{1}{\sqrt{8 \frac{C}{N_0} B R_c}} \quad \text{for} \quad \frac{B}{R_c} \rightarrow \infty \quad (3.12)$$

Finally, a lower and an upper bound for the exact solution are given by the boundaries for $n=1$ and $n \rightarrow \infty$:

$$\sigma_{\tau,1} \leq \sigma_{\tau} \leq \sigma_{\tau,\infty} \quad (3.13)$$

$$\frac{0.3359}{\sqrt{\frac{C}{N_0} B R_c}} \leq \sigma_{\tau} \leq \frac{0.3536}{\sqrt{\frac{C}{N_0} B R_c}} \quad (3.14)$$

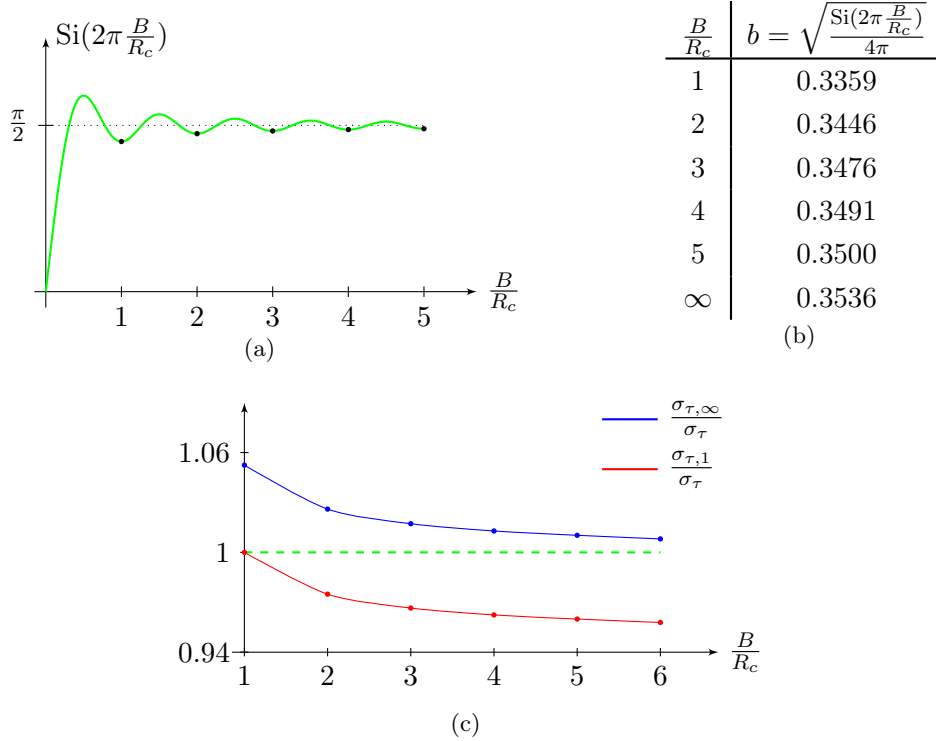


Figure 3.3: Approximation for rectangular pulses: (a) The Si function, (b) the numerators for integer values of $\frac{B}{R_c}$, (c) the exact solution inside its two boundaries.

In the GPS system, rectangular pulses are used in the C/A code with a chiprate $R_c=1.023$ MHz. A comparison of my results of the Ramer Rao lower bound for rectangular pulses to the result from [4] for the GPS C/A code in Eq. (3.15) proofs the derivation, whereas the numerator differs by a small amount from my approximations.

$$\sigma_r \geq \underbrace{\frac{3.444 \cdot 10^{-4}}{\sqrt{\frac{C}{N_0}} B}}_{[4]} = \frac{0.3483}{\sqrt{\frac{C}{N_0}} B R_c} \quad (3.15)$$

3.3.2 Root raised cosine pulses

For root raised cosine pulses, the square of the magnitude of the Fourier transform, that is needed for the calculation of the Cramer Rao lower bound, is the Fourier transform of the raised cosine pulse:

$$|S_m(f)|^2 = \begin{cases} T_c & |f| \leq (1 - \alpha) \frac{1}{2T_c} \\ \frac{T_c}{2} \left[1 - \sin\left(\frac{T_c}{2\alpha}(2\pi|f| - \frac{\pi}{T_c})\right) \right] & (1 - \alpha) \frac{1}{2T_c} \leq |f| \leq (1 + \alpha) \frac{1}{2T_c} \\ 0 & |f| \geq (1 + \alpha) \frac{1}{2T_c} \end{cases} \quad (3.16)$$

For root raised cosine pulses with a common bandwidth B, the chip duration T_c is substituted:

$$T_c = (1 + \alpha) \frac{1}{2B} \quad (3.17)$$

and the limits are:

$$B_1 = (1 - \alpha) \frac{1}{2T_c} = B \frac{(1 - \alpha)}{(1 + \alpha)} \quad \text{and} \quad B_2 = (1 + \alpha) \frac{1}{2T_c} = B \quad (3.18)$$

The Fourier transform of the raised cosine pulse as a function of the frequency f is then:

$$|S_m(f)|^2 = \begin{cases} T_c & |f| \leq B_1 \\ \frac{T_c}{2} \left[1 - \sin\left(\frac{T_c}{2\alpha}(2\pi|f| - \frac{\pi}{T_c})\right) \right] & B_1 \leq |f| \leq B \\ 0 & |f| \geq B \end{cases} \quad (3.19)$$

Since a normalized version of the raised cosine pulse is used, the pulse energy is:

$$\begin{aligned} \int_{-B}^B |S_m(f)|^2 df &= 2T_c \int_0^{B_1} df + T_c \int_{B_1}^B \left[1 - \sin\left(\frac{T_c}{2\alpha}(2\pi f - \frac{\pi}{T_c})\right) \right] df \\ &= 2T_c f \Big|_0^{B_1} + T_c \left[f + \frac{\alpha}{\pi T_c} \cos\left(\frac{2fT_c\pi - \pi}{2\alpha}\right) \right] \Big|_{B_1}^B \\ &= (1 - \alpha) + \frac{1 + \alpha}{2} - \frac{1 - \alpha}{2} + \frac{\alpha}{\pi} \cos\left(\frac{(1 + \alpha)\pi - \pi}{2\alpha}\right) - \frac{\alpha}{\pi} \cos\left(\frac{(1 - \alpha)\pi - \pi}{2\alpha}\right) \\ &= 1 + \frac{\alpha}{\pi} \cos\left(\frac{\pi}{2}\right) + \frac{\alpha}{\pi} \cos\left(-\frac{\pi}{2}\right) = \underline{1} \end{aligned} \quad (3.20)$$

and

$$\begin{aligned}
\int_{-B}^B f^2 |S_m(f)|^2 df &= 2T_c \int_0^{B_1} f^2 df + T_c \int_{B_1}^B f^2 \left[1 - \sin \left(\frac{T_c}{2\alpha} (2\pi f - \frac{\pi}{T_c}) \right) \right] df \\
&= \frac{2}{3} T_c f^3 \Big|_0^{B_1} + \frac{1}{3} T_c f^3 + \frac{\alpha}{T_c^2 \pi^3} \left((f^2 T_c^2 \pi^2 - 2\alpha^2) \cos \left(\frac{2f T_c \pi - \pi}{2\alpha} \right) \right) \\
&\quad - \frac{\alpha}{T_c^2 \pi^3} \left(2f \alpha T_c \pi \sin \left(\frac{2f T_c \pi - \pi}{2\alpha} \right) \right) \Big|_{B_1}^B \\
&= \frac{2}{3} T_c B_1^3 + \frac{1}{3} T_c B^3 - \frac{1}{3} T_c B_1^3 \\
&\quad + \frac{\alpha}{T_c^2 \pi^3} \left(\frac{(1+\alpha)^2 \pi^2}{4} - 2\alpha^2 \right) \cos \left(\frac{(1+\alpha)\pi - \pi}{2\alpha} \right) \\
&\quad - \frac{\alpha}{T_c^2 \pi^3} \left(\frac{(1-\alpha)^2 \pi^2}{4} - 2\alpha^2 \right) \cos \left(\frac{(1-\alpha)\pi - \pi}{2\alpha} \right) \\
&\quad - \frac{\alpha}{T_c^2 \pi^3} \left(\frac{(1+\alpha)2\pi\alpha}{2} \right) \sin \left(\frac{(1+\alpha)\pi - \pi}{2\alpha} \right) \\
&\quad + \frac{\alpha}{T_c^2 \pi^3} \left(\frac{(1-\alpha)2\pi\alpha}{2} \right) \sin \left(\frac{(1-\alpha)\pi - \pi}{2\alpha} \right) \\
&= \frac{1}{3} T_c B_1^3 + \frac{1}{3} T_c B^3 + \frac{\alpha}{T_c^2 \pi^3} \left(\frac{(1+\alpha)^2 \pi^2}{4} - \frac{(1-\alpha)^2 \pi^2}{4} - 4\alpha^2 \right) \cancel{\cos \left(\frac{\pi}{2} \right)}^0 \\
&\quad + \frac{\alpha}{T_c^2 \pi^3} \left(-\frac{2\pi\alpha(1+\alpha)}{2} - \frac{2\pi\alpha(1-\alpha)}{2} \right) \cancel{\sin \left(\frac{\pi}{2} \right)}^1 \\
&= \frac{B^2}{6} \frac{(1-\alpha)^3}{(1+\alpha)^2} + \frac{B^2(1+\alpha)}{6} + \frac{\alpha(-\pi\alpha(1+\alpha) - \pi\alpha(1-\alpha))}{T_c^2 \pi^3} \\
&= B^2 \left[\frac{(1-\alpha)^3 + (1+\alpha)^3}{6(1+\alpha)^2} - \frac{8\alpha^2}{\pi^2(1+\alpha)^2} \right] \\
&= B^2 \left[\frac{1+3\alpha^2}{3(1+\alpha)^2} - \frac{8\alpha^2}{\pi^2(1+\alpha)^2} \right]
\end{aligned} \tag{3.21}$$

The Cramer Rao lower bound for root raised cosine pulses finally is:

$$\boxed{\sigma_\tau \geq \frac{1}{\sqrt{8\pi^2 \frac{C}{N_0} B^2 f(\alpha)}} \quad \text{with} \quad f(\alpha) = \frac{1+3\alpha^2}{3(1+\alpha)^2} - \frac{8\alpha^2}{\pi^2(1+\alpha)^2}} \tag{3.22}$$

3.4 Discussion

The results from the last section showed that the influence of white noise depends on the signal-to-noise ratio and on the shape of the transmit pulse. For both types of pulses, the shape is determined by two parameters, whereas the bandwidth is the only common parameter.

Bandlimited rectangular pulses

An approximation for the mean error for bandlimited rectangular pulses is:

$$\sigma_\tau \geq \frac{\text{const.}}{\sqrt{\frac{C}{N_0} B R_c}} \quad (3.23)$$

The mean error depends on the bandwidth and the chiprate in the same way, increasing one of the two parameters will reduce the mean error, whereas the ratio of the bandwidth to the chiprate should always be greater than one to maintain the rectangular shape (see Figure 2.6 and Figure 2.7). Doubling any of the two parameters reduces the error by 3 dB.

Root raised cosine pulses

The exact solution of the lower bound for root raised cosine pulses is:

$$\sigma_\tau \geq \frac{1}{\sqrt{8\pi^2 \frac{C}{N_0} B^2 f(\alpha)}} \quad \text{with} \quad f(\alpha) = \frac{1 + 3\alpha^2}{3(1 + \alpha)^2} - \frac{8\alpha^2}{\pi^2 (1 + \alpha)^2} \quad (3.24)$$

The mean error depends on the bandwidth and the roll-off factor, whereas the smallest error for a given bandwidth is achieved for a roll-off factor $\alpha = 0$, where the pulse is shorter than for $\alpha > 0$. The difference to a roll-off factor of 1 is ≈ 4 dB. Doubling the bandwidth reduces the error by 6 dB (9 dB if the other definition of the signal-to-noise ratio is used), the same result as for rectangular pulses, if both, the bandwidth and the chiprate are doubled.

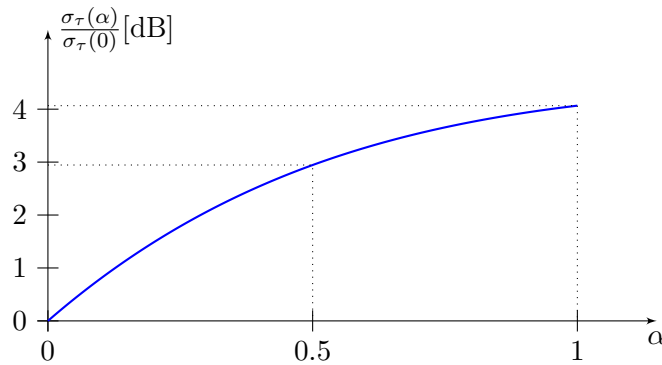


Figure 3.4: Standard deviation for root raised cosine pulses.

Comparison

Figure 3.5 shows the mean error of root raised cosine pulses and rectangular pulses with a fixed chiprate as a function of the bandwidth. For bandwidths higher than the chiprate, a raised cosine pulse is better than a rectangular pulse. The gain increases with higher values of the bandwidth.

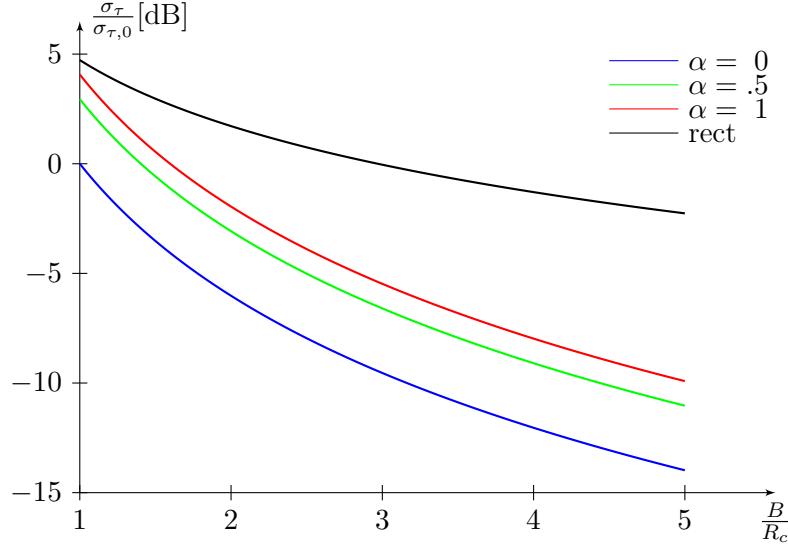


Figure 3.5: Comparison of rectangular and root raised cosine pulses.

Even though for a given $\frac{C}{N_0}$ the total noise power inside the transmission bandwidth is proportional to the bandwidth, the mean error decreases for an increasing bandwidth.

3.4.1 The observation time

In the last section, the mean error was calculated as a function of the signal-noise-ratio $\frac{C}{N_0}$, the ratio of the symbol energy to the noise power spectral density, whereas the symbol energy can be expressed as the mean signal power multiplied by the length of one symbol. Thus, the Cramer Rao lower bound is also a function of the symbol length. In order to take account of the symbol length, the other definition of the signal-to-noise ratio is used, where the Cramer Rao lower bound is indirectly proportional to the square-root of the symbol length:

$$\sigma_\tau \sim 1/\sqrt{\text{SNR} \cdot T_D} \quad (3.25)$$

In common direct sequence spread spectrum systems, the symbol length T_D is the length of one period of the spreading sequence, $T_D = \frac{L}{R_c}$ (the length of one period of the spreading sequence in chips divided by the chiprate). Whereas in correlation receivers, T_D equals the integration time, in matched filter receivers, the length of the impulse response of the matched filter is T_D , thus, T_D may also be termed "observation time".

Increasing the observation time

In order to reduce the mean error, the symbol length should be as long as possible. This can be achieved during the design of the system by using a longer spreading sequence or a lower chiprate, which will both result in a lower symbol rate. For a given symbol length, the mean error may also be reduced by increasing the observation time in the receiver.

To increase the observation time in the receiver, two techniques were found in [3]:

- **Coherent summation:** If the transmit signal is just a periodic sequence of the spreading sequence (no data is transmitted), the phase of the received signal is constant and thus the integration time of the receiver may be increased to any desired value.
- **Noncoherent summation:** If data is transmitted, the data symbols are usually not known in advance, so the coherent summation would only work if the data symbols were known. For this case, the mean error can be reduced by calculating the correlation over one symbol length, saving the result of the correlation and adding the squared magnitudes of N saved correlations:

$$\widetilde{ccf}(\tau) = \sum_{n=1}^N |ccf_n(\tau)|^2 \quad (3.26)$$

The estimation of the position is then done by maximizing $\widetilde{ccf}(\tau)$.

Simulations showed that both techniques reduce the mean error in the same way. For every doubling of the observation time, or doubling of N, the mean error is reduced by 3 dB. The only difference is the minimum signal-to-noise ratio mentioned in Section 3.2, while the minimum SNR for coherent summation is reduced by 3 dB for every doubling of the observation time, it is only reduced by ≈ 2 dB for noncoherent summation.

Calculating the mean

The mean error may also be reduced by calculating the mean over a certain number of results:

$$\hat{\tau} = \frac{1}{N} \sum_{n=1}^N \hat{\tau}_n \quad (3.27)$$

Simulations showed, that the standard deviation of the mean position $\hat{\tau}$ is reduced in the same way as the observation time was increased from T to N·T, with the difference, that the minimum signal-to-noise ratio remains the same as for the single estimations $\hat{\tau}_n$.

Chapter 4

Multipath propagation

In wireless communication systems, the transmit signal reaches the antenna by more than one path due to the reflection from objects such as buildings and cars, called multipath propagation. According to the different propagation times along the different paths, the signals arrive with different delays at the receiving antenna (see Figure 4.1).

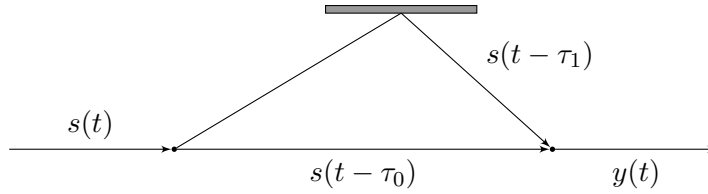


Figure 4.1: Multipath propagation.

For N paths, the impulse response of a static multipath channel is:

$$h(t) = \sum_{n=0}^{N-1} a_n e^{j\phi_n} \delta(t - \tau_n) \quad (4.1)$$

with the Fourier transform:

$$H(j\omega) = \int_{-\infty}^{\infty} h(t) e^{-j\omega t} dt = \sum_{n=0}^{N-1} a_n e^{j\phi_n} e^{-j\omega \tau_n} \quad (4.2)$$

where τ_n is the propagation time, a_n the amplitude and ϕ_n the phase of the n-th path. This very simple model of a multipath channel does not take account of the effect of doppler shift due to moving receivers and transmitters.

4.1 Ranging errors due to multipath propagation

In all positioning and ranging applications, the line-of-sight path, the path where no reflections occur is the desired path. Due to reflections, all other signals reach the receive antenna later than the line-of-sight signal and cause errors in the estimation of the propagation time of the desired line-of-sight signal. Figure 4.2 shows the received pulse for a simple model with one secondary path and no phase difference:

$$h(t) = a\delta(t - \tau_0) + a_1\delta(t - \tau_1) \quad (4.3)$$

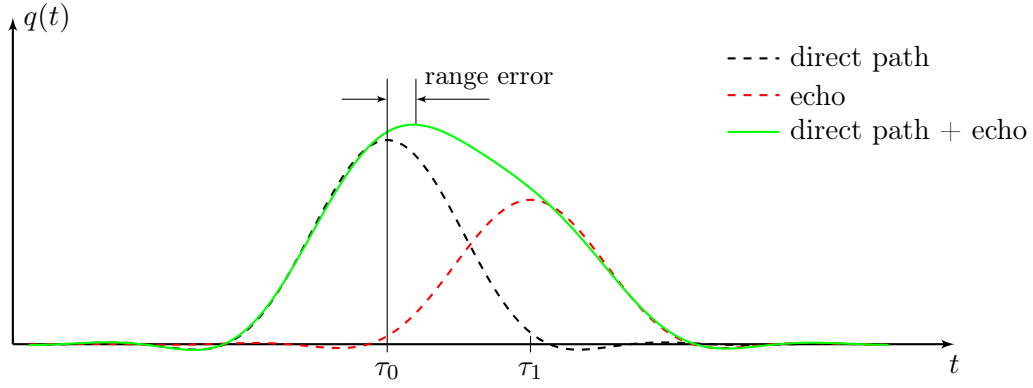


Figure 4.2: Ranging errors due to multipath propagation.

The result is a distorted pulse having its maximum at a different time as the undistorted line-of-sight pulse. The influence of the transmit pulse and the channel parameters onto this error is simulated in the following.

4.2 Simulation

For the simulation of the influence of a multipath channel onto the estimation of the propagation time, a very simple channel model consisting of the line-of-sight and one echo path was used. With the normalization of the line-of-sight path to an attenuation of 1 and a phase of 0, the impulse response of the channel filter is:

$$h(t) = \delta(t) + ae^{j\phi}\delta(t - \Delta\tau) \quad \text{with} \quad a < 1 \quad (4.4)$$

with a propagation time difference $\Delta\tau$ between the line-of-sight and the echo path.

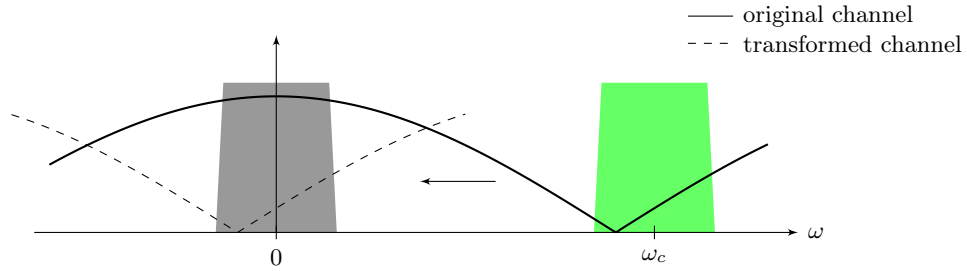


Figure 4.3: Multipath propagation in the passband: For the simulation in the baseband, the channel filter has to be transformed into the baseband.

An additional phase is introduced by the passband to baseband transformation of the received signal. Since the transmit signal passes the channel filter in the passband, the simulation has to be done in the passband or the channel filter has to be shifted to the baseband. For the second option, the equivalent baseband impulse response of the channel filter for a carrier frequency of ω_c is:

$$h(t) = \delta(t) + ae^{j\phi}e^{-j\omega_c\Delta\tau}\delta(t - \Delta\tau) \quad (4.5)$$

In the following simulations, the difference of the estimated signal delay $\hat{\tau}$ to the signal delay τ for the undistorted line-of-sight path was determined for different pulses, whereas only the worst case was simulated. This worst case is given by a total phase $(\phi - \omega_c \Delta\tau)$ of 0 and π , where the two received signals are in phase or in opposite phase. Figure 4.4 shows, that the error for other values of the phase are all inside an envelope given by the error for $\phi = 0, \pi$ and $\omega_c = 0$. The power of the echo was set to $a = -3$ dB in all simulations.

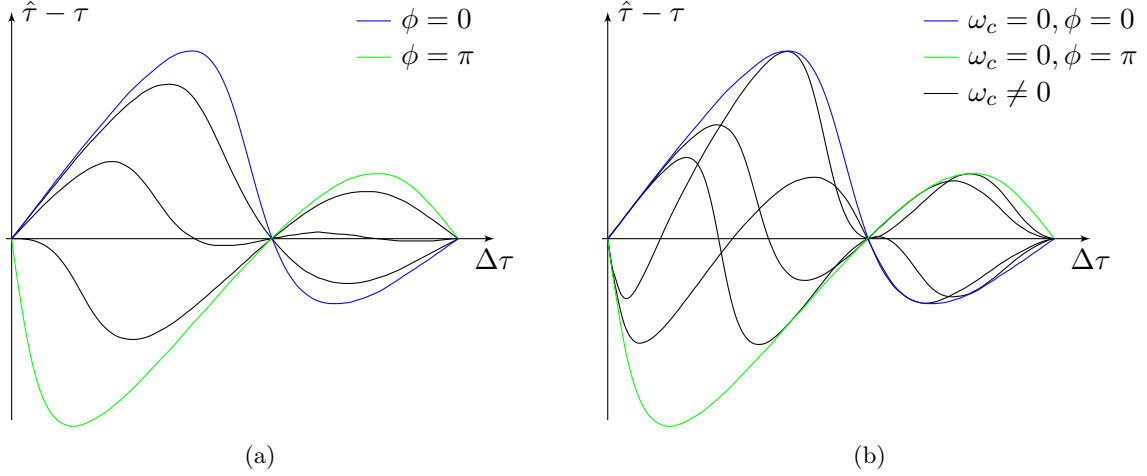


Figure 4.4: Multipath error as a function of the phase: (a) for $\omega_c = 0$ and different values of ϕ . (b) for different values of ω_c .

4.2.1 Rectangular pulses

The shape of bandlimited rectangular pulses is given by the chiprate and the bandwidth. For a certain chiprate the error is the smaller, the higher the bandwidth. While for bandwidths higher than ≈ 4 times the chiprate, multipath errors are limited to time differences $\Delta\tau$ smaller than the chiplength T_c , for smaller bandwidths, there are evident errors for higher time differences (see Figure 4.5 (a)).

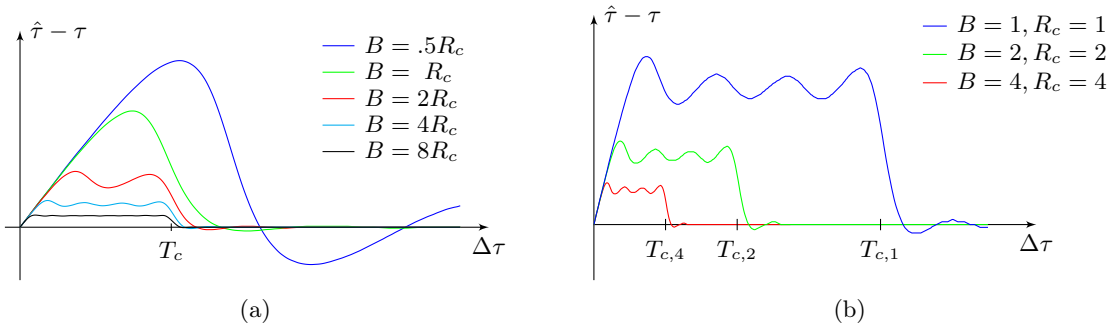


Figure 4.5: Multipath error for rectangular pulses: (a) for a given chiprate. (b) for constant ratios of the bandwidth to the chiprate.

For constant ratios of the bandwidth to the chiprate, the multipath error reduces to the half for every doubling of the chiprate and the bandwidth, as well as the maximum time difference where errors occur is reduced to the half (see Figure 4.5 (b)).

4.2.2 Root raised cosine pulses

The shape of root raised cosine pulses is determined by the bandwidth and the roll-off factor, for a certain bandwidth the pulsewidth is the higher, the higher the roll-off factor. This higher pulsewidth results in an higher maximum error and a shift of the maximum to higher time differences $\Delta\tau$. On the other hand, the (effective) impulse response of root raised cosine pulses is the shorter, the higher the roll-off factor. While the error for a roll-off factor of 1 is limited to time differences lower than \approx the pulsewidth, the influence for lower roll-off factors is still evident for much higher time differences. (see Figure 4.6 (b)).

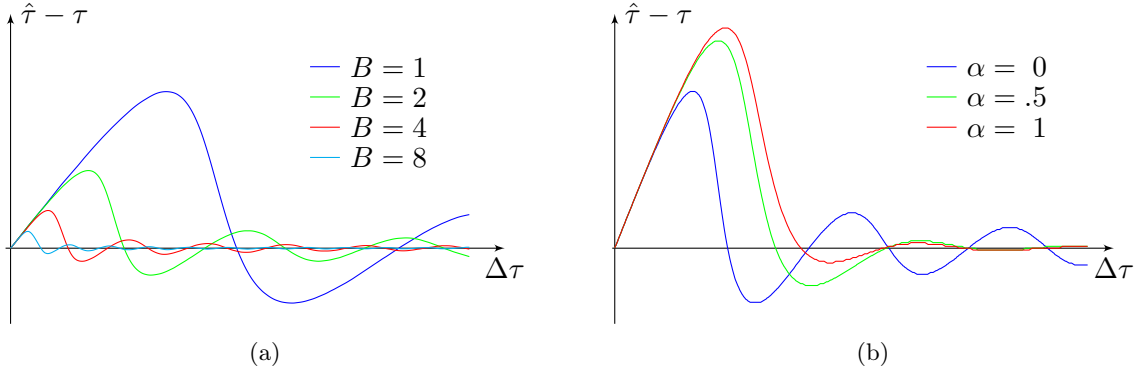


Figure 4.6: Multipath error for root raised cosine pulses: (a) for different values of the bandwidth. (b) for different roll-off factors.

Figure 4.6 (a) shows the error for different values of the bandwidth, independent of the roll-off factor, a higher bandwidth results in lower errors and an compression of the error characteristic.

4.2.3 Comparison

In order to compare the different pulses, the results for the maximum bandwidth of the system described in Chapter 5 were used. These results are shown in Figure 4.7 where a propagation speed of $c_0 \approx 3 \cdot 10^8$ m/s was assumed and both, the time differences as well as the errors, were multiplied by c_0 . The length of one chip is then ≈ 6 m.

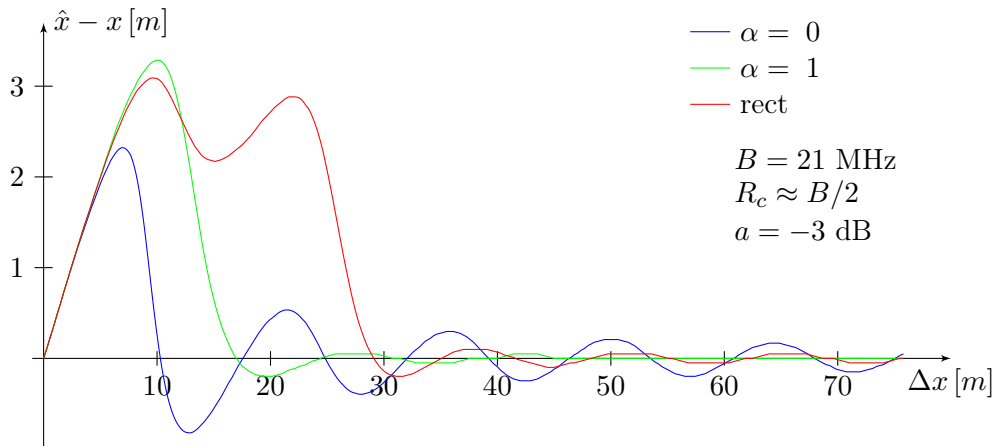


Figure 4.7: Multipath errors in comparison of different pulses.

The largest errors occur for rectangular pulses and raised cosine pulses with a roll-off factor of $\alpha = 1$, while the lowest error is obtained for sinc pulses. On the other hand, the higher the distance difference, the worse the sinc pulses compared to rectangular and raised cosine pulses with higher roll-off factors are, where significant errors only occur for distance differences lower than a certain bound (≈ 30 m in Figure 4.7).

In Figure 4.7, the used chiprate of $\approx B/2$ is a tradeoff between a limitation of the error to quite low distance differences and low errors for distance differences above this bound. Reducing the chiprate would lower the error above the bound, while the bound is shifted to the right. Higher chiprates would result in lower errors for small distance differences, but larger errors for higher distance differences.

Chapter 5

The measurement system

In this chapter the measurement system i set up at the institute is introduced. It consists of a single transmitter and a single receiver hardware unit fully controlled by MATLAB.

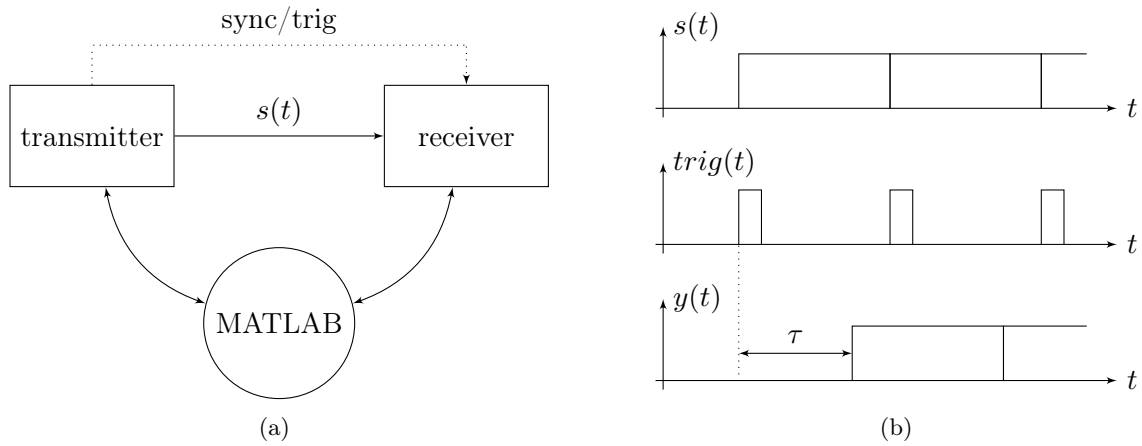


Figure 5.1: Measurement system: (a) block diagram. (b) synchronization of transmitter and receiver using a trigger.

A periodic transmit signal $s(t)$ is send to the receiver, where the signal is demodulated and the time difference between the arrival of the signal and the arrival of the trigger is estimated. Therefore, a trigger signal $trigg(t)$, that is generated in the transmitter, periodically initiates the recording of data in the receiver. This periodic estimation of the propagation delay makes it possible to repeat every measurement as often as needed to calculate the mean error caused by interferers.

In the design of the system, the following requirements had to be implemented:

- The power and the frequency of the transmit signal can be set to an arbitrary value.
- The baseband signals can be complex valued. Therefore, both, the transmitter and the receiver must be able to handle complex signals.
- The generation of the transmit signals as well as the processing of the received signals is done in MATLAB in the same way as in the simulations.
- The transmit signal may optionally by modulated with data.
- The transmit signal is directly loaded via MATLAB to the transmitter, and the received signal is directly copied from the receiver back to MATLAB.
- The configuration of all devices is done in MATLAB.

5.1 Transmitter

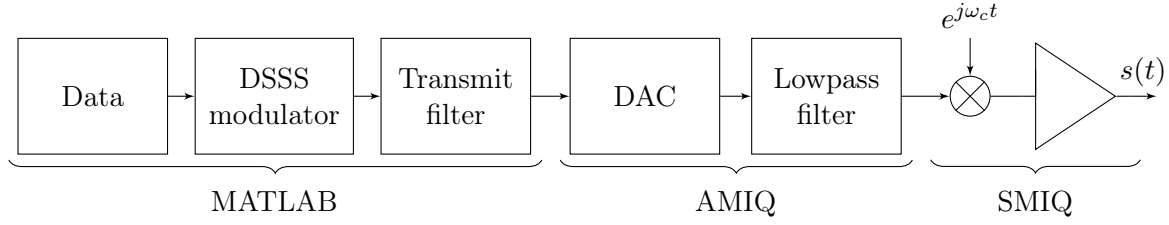


Figure 5.2: Transmitter.

The transmitter consists of three parts:

- **MATLAB:** Generation of one period of the baseband signal.
- **AMIQ:** Periodic output of the baseband signal generated in MATLAB.
- **SMIQ:** Amplification and modulation onto the desired carrier frequency.

5.1.1 The AMIQ signal generator

The AMIQ signal generator [5] is a modulation source that uses two synchronous DACs to generate complex valued baseband signals. The two output signals, the in-phase (real part) and the quadrature (imaginary part) component, are usually connected to the two modulation inputs of a modulator which modulates the signal onto the desired carrier frequency. Parallel to the two signal outputs the AMIQ also provides four user programmable digital marker outputs which operate synchronously to the signal outputs. A marker output can be used to trigger a measurement.

Specifications

- 14 bit resolution
- 10 Hz ... 100 MHz sample rate
- For the reconstruction filter a cut-off frequency of 2.5 Mhz, 25 MHz, or no filtering can be chosen.
- The maximum output voltage is $0.5 V_p$ into a 50Ω load.
- Markers are TTL

Sinc distortion

The outputs of the AMIQ's DACs are "zero order hold" that hold the voltage constant for an update period $T_s = 1/f_s$. In the frequency domain, this zero order hold introduces $\sin(x)/x$ distortion. Figure 5.3 shows the output signal spectrum is multiplied by the transfer function given by Eq. (5.1). Thus, the sinc distortion acts like a low pass filter that attenuates image frequencies, but also attenuates the desired in-band signals.

$$H(j\omega) = \text{sinc}\left(\pi \frac{\omega}{\omega_s}\right) = \frac{\sin\left(\pi \frac{\omega}{\omega_s}\right)}{\pi \frac{\omega}{\omega_s}} \quad (5.1)$$

For an update rate of $f_s = 47.5$ MHz (the external sample rate of the receiver) the attenuation at the maximum signal frequency of 21 MHz (see Section 6.2 for the determination of the maximum bandwidth) is ≈ 3 dB.

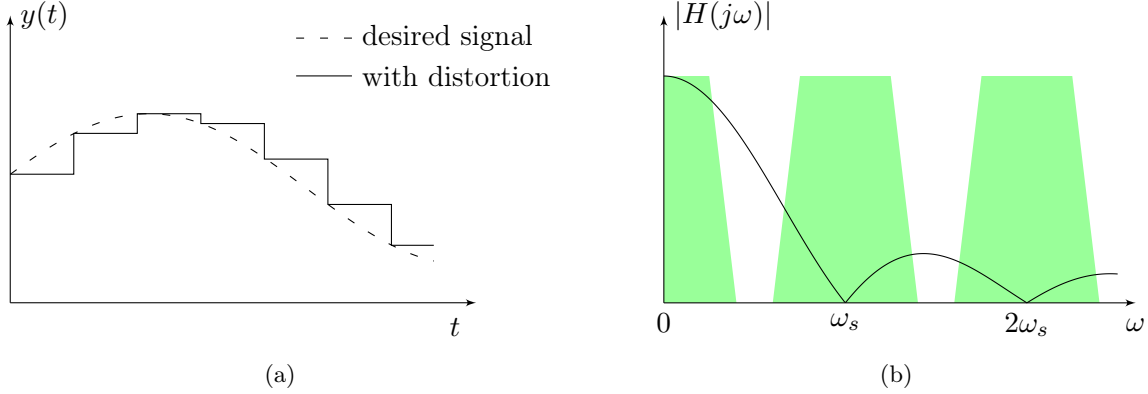


Figure 5.3: Sinc distortion: (a) DAC output signal. (b) Attenuation in the frequency domain.

Four techniques to reduce or eliminate this effect were found in [6]:

- **Increasing the update rate (oversampling):** Since the DAC's output attenuation depends on its update rate, the effect of sinc rolloff can be minimized by increasing the update rate and keeping the signal bandwidth unchanged. Increasing the update rate not only reduces the effect of non flat frequency response, it also lowers the quantization noise floor and loosens requirements for the reconstruction filter.
- **Interpolation in the DAC:** Interpolation DACs include one or more digital filters, which insert a sample after each existing data sample with a value interpolated between each pair of consecutive data sample values. This technique increases the update rate while keeping the data rate at lower frequency.
- **Pre equalization:** Increasing the update rate reduces but does not eliminate the effect of sinc frequency rolloff. It is possible to design a digital filter whose frequency response is the inverse of the sinc function. Such a pre-equalization filter filters the digital input data to equalize the signal, and then sends the data to the DAC. It allows the original signal to be reconstructed without attenuation, while the dynamic of the resulting output signal is reduced due to the pre-amplification.
- **Post equalization:** As an alternative to the pre equalization, an analog (post equalization) filter whose frequency response is approximately equal to the inverse of the sinc function may be used. This filter is inserted after the DAC's reconstruction filter.

For the DACs in the AMIQ, only pre equalization and increasing the update rate are useful techniques to reduce or eliminate the sinc distortion. When using given DACs, like the ones in the AMIQ, an interpolation can only be achieved by increasing the data rate and the update rate in the same way and keeping the bandwidth unchanged. Post equalization requires additional hardware that has to be changed whenever the update rate changes, while a digital pre equalization filter is independent of the update rate.

- The **pre equalization filter** was designed in MATLAB using the *fir2* function that generates FIR filters with arbitrarily shaped frequency responses using a frequency sampling based design.

```
f=(0:0.01:1);
m=1./sinc(f/2);
b=fir2(100,f,m);
x_equ=filter(b,1,x);
```

- **Increasing the update rate** from 47.5 MHz to an update rate of 95 MHz that is used in Section 5.3, reduces the attenuation to ≈ 0.7 dB at 21 MHz

Communication with MATLAB

The remote configuration of AMIQ and the transmission of the signal waveforms to AMIQ is done via the GPIB¹ bus.

To load a new waveform into the AMIQ, the following has to be done:

1. Filter the signal with the pre equalization filter to eliminate the sinc distortion.
2. Scale the signal to the full scale of the DACs to achieve the maximum dynamic of 14 bit.
3. Combine the two 14 bit signal samples and the four 1 bit marker samples to two 16 bit words.
4. Open a connection to AMIQ.
5. Reset AMIQ.
6. Choose the sample rate.
7. Choose if AMIQ should synchronize to an external 10 MHz reference.
8. Choose the reconstruction filter (2.5 MHz, 25 MHz, external or off).
9. Copy the signal to AMIQ.
10. Activate the marker outputs.
11. Activate the in-phase and quadrature outputs and choose the mode. For an operation with the SMIQ modulator the mode *FIX* should be used.
12. Choose the desired trigger. For a continuous operation, a software trigger will start the output.
13. Close the connection to AMIQ.

¹General Purpose Instrumentation Bus, IEEE 488

5.1.2 The SMIQ vector modulator

The SMIQ vector modulator [7] modulates the (complex valued) baseband signal generated by AMIQ to the desired carrier frequency and amplifies it.

In the version of SMIQ that was used:

- a carrier frequency between 300 kHz and 6.4 GHz can be used.
- the (peak) transmit power can be between $-140 \dots +10$ dBm.

To transmit with a certain RMS² power instead of a certain peak power, the crest-factor³ of the baseband signal can be send to SMIQ. It is then automatically added to the desired power.

The communication with MATLAB works the same way as with AMIQ. After sending a reset and switching to the *vector modulation mode*, the desired carrier frequency, the transmit power and optionally the crest factor can be send. The connection to SMIQ then can be closed. If any of the paramteres needs to be changed during operation, a new connection can be established without resetting the SMIQ.

5.2 Receiver

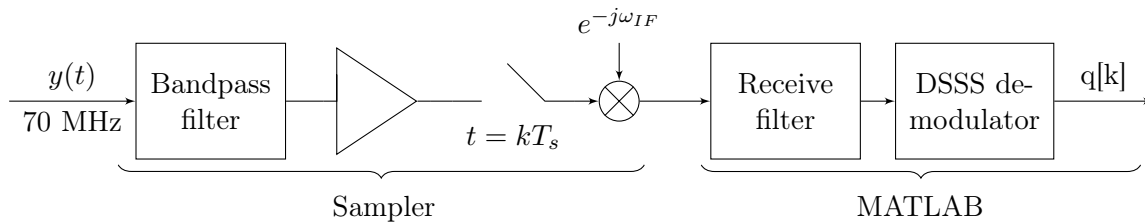


Figure 5.4: Receiver.

The receiver consists of two parts:

- **Sampler:** Amplification, sampling, and digital downconversion to the baseband.
- **MATLAB:** Filtering, demodulation and all further processing.

While the transmitter described in the last section is ready for use at typical radio frequencies, the receiver only works for signal at an intermediate frequency of 70 MHz. For measurements at typical radio frequencies an additional downconverter is needed.

5.2.1 The 70 MHz IF sampler

The sampler that is used as receiver is the *Agilent E1439 VXI 70 MHz IF sampler* [8] with a maximum sample rate of 95 MSa/s. In the IF mode, both, the in-phase and the quadrature

²Root-Mean-Square

³The baseband definition of the crest factor is the ratio of the peak to the average of a signal, $c_x = \frac{|x|_{max}}{\sqrt{P_x}}$

component of the received signal are converted to the baseband (passband to equivalent baseband transformation) using a single sampler, whereas the phase of the resulting baseband signal varies from measurement to measurement, it can be estimated and corrected in MATLAB.

In common applications of the sampler, two modules are used, an input module and the sampler module. While the sampler module and its remote control is well documented, no information about the input module was found. Hence, the input module was not used and the input signal was directly sent to the sampler module.

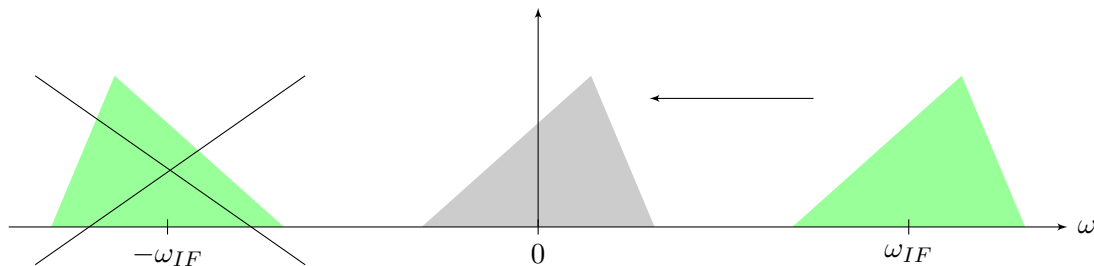


Figure 5.5: Passband to baseband transformation.

The remote control and the transmission of the sampled signals via the firewire⁴ bus to the workstation is done using VISA⁵. Therefore, a software library (DLL), that provides all the functions to communicate with the sampler, has to be loaded into MATLAB.

Configuration of the sampler

For the use in the measurement system, the following settings have to be considered:

- **Input signal path:** Whether to use the baseband or the 70 MHz IF path.
- **Clock setup:** Depending on the application, different sources for clocking and synchronization can be used. The following predefined configurations were used (see Section 5.3):
 - internal sample clock of 95 MHz and no synchronization.
 - internal sample clock of 95 MHz and synchronization to an external 10 MHz reference.
 - external sample clock.
- **Data mode:** Whether data shall be collected in continuous mode or in block mode. For triggered measurements the block mode is used, where an external trigger starts the collection of a block of data and the measurement is halted until the data is send to the workstation.
- **Blocksize:** The size of one block of data.
- **Resolution:** The resolution of the sampler can be set to 12 or 24 bit. Because of the broadband white noise present on the input of the ADC, the sampler is limited to 12 bit resolution for input bandwidths greater than 10 MHz.

⁴IEEE 1394

⁵Virtual Instrument Software Architecture

- **Spectral order:** The spectrum of the output data can be in the same spectral order as the input signal or in the reverse order.
- **Bandwidth:** The 3 dB input bandwidth can be adjusted to $B = 0.44f_s/2^{\text{sigBw}}$, where f_s is the sample frequency and sigBw is (when using the IF path) an integer value > 0 , where for sigBw=1, the maximum (one-sided) bandwidth is 20.9 MHz.
- **Decimation:** The sampler automatically decimates every output signal to a data rate of $f_s/2^{\text{sigBw}-1}$. Optionally, an extra decimation by a factor of two can be made. For the highest input bandwidth of 20.9 MHz, the optional decimation has to be used, the output data rate is then 47.5 MSa/s.
- **Trigger:** The start of collecting data can be triggered by different internal and external trigger events. For the triggered measurements in combination with the transmitter described in Section 5.1, external triggering with TTL level transition is used.
- **Input range:** In the IF mode, the input range of the sampler can be set in 1 dB steps to values from -36 to +12 dBm. There is also an auto ranging mechanism that sets the input range to the lowest value that does not cause an ADC overload.

The measurement procedure

After the initialization and configuration of the sampler, the collection of one block of data is invoked by sending a command to arm the trigger. The sampler will start collecting data when the next hardware trigger occurs. The block of data that was saved can then be copied to MATLAB. For the next block of data, a new software trigger has to be send.

For every measurement, the sampler provides following additional information:

- The **actual trigger delay:** This is the delay, measured in periods of the ADCs sample clock between the time the trigger occurred and the first sample was taken. The trigger delay varies from block to block, so it needs to be taken in account. See Section 5.3 for more information.
- The **actual phase:** This is the phase of the internal LO⁶ at the time the trigger occurred.
- The **overload bit:** This indicates if there was an overload at the input of the sampler when the block of data was sampled.

⁶Local oscillator

5.2.2 Equalization

The simulations in the previous chapters showed that the bandwidth is a very important signal parameter for the precision of positioning systems. Hence, the signals in the measurement system should be transmitted with the highest possible bandwidth. In the described measurement system the bandlimiting device is rather the receiver than the transmitter. While the sampler's maximum 3 dB bandwidth is ≈ 21 MHz, the transmitter can generate signals with a bandwidth of up to ≈ 25 MHz (if a reconstruction filter is used).

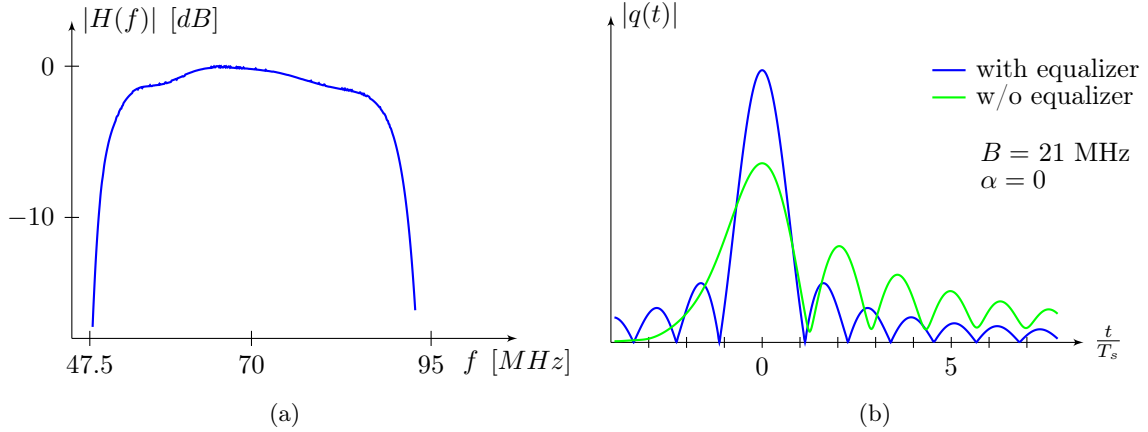


Figure 5.6: Sampler input characteristic: (a) Frequency response. (b) Response to a raised cosine pulse.

Figure 5.6 illustrates the measured distortion that is introduced by the samplers input filters, and even for bandwidths much smaller than 21 MHz, the samplers frequency response is not flat. In order to transmit with the highest possible bandwidth and to obtain the desired output pulses in the receiver, an equalizer was designed.

Zero forcing equalizer design

Zero forcing equalizers [2] remove all the distortion by multiplying the received signal with the inverse of the channel transfer function. Therefore the channel transfer function $H(j\omega)$ has to be known.

$$D_{ZF}(j\omega) = \frac{1}{H(j\omega)} = \frac{X(j\omega)}{Y(j\omega)} \quad (5.2)$$

While the influence of the channel completely vanishes, the great disadvantage of the zero forcing equalizer is its effect on noise. Values of the channel transfer function $H(j\omega)$ near zero will result in a significant noise amplification. In case of the input filters of the sampler, this is at frequencies higher than ≈ 21 MHz. See Section 6.2 for an illustration of the noise amplification.

For the calculation of the sampler input equalizer, the FFT transform of one period of the transmit signal is divided by the FFT transform of one period of the received signal.

5.3 Synchronization

In unsynchronized operation, where the transmitter and the receiver generate their own sample clocks, the trigger arrives at the receiver with an unknown and varying time difference to the next sample pulse. While the trigger delay in the receiver (see Section 5.2.1) can be compensated by shifting the estimated signal position to the left, the time difference between the arrival of the trigger and the next sample is unknown.

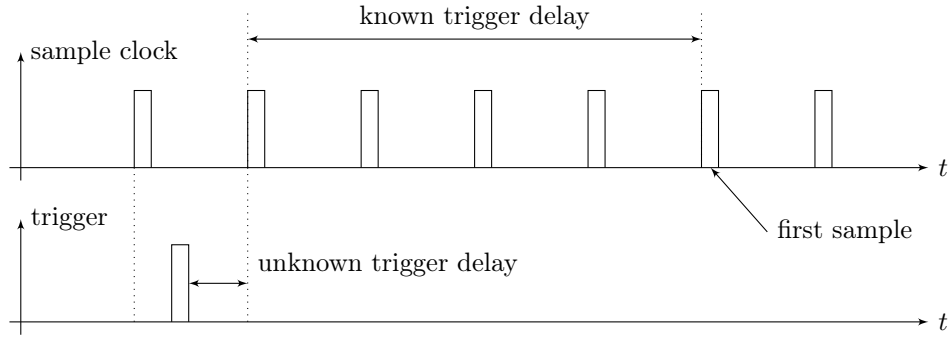


Figure 5.7: Known and unknown trigger delay.

Figure 5.8 shows the results of a continuous measurement of the signal position, whereas Δx is the difference between the estimated position and the mean position. For the unsynchronized case, the estimated position is equally likely distributed within one sample period⁷. This results in a mean positioning error of ≈ 0.9 m, which is much too large for making useful measurements.

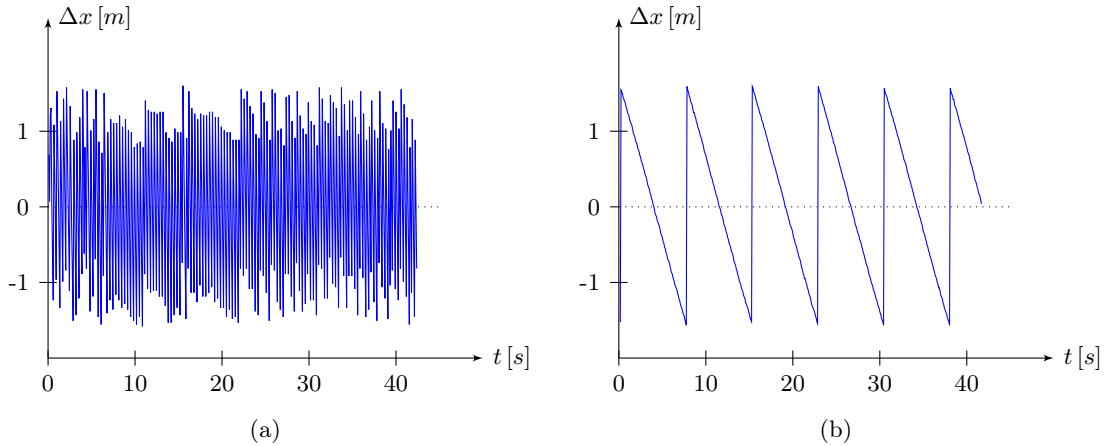


Figure 5.8: Continuous estimation of the signal position: (a) No synchronization. (b) Synchronization via the 10 MHz reference.

⁷For free space propagation and a sample frequency of 95 MHz one sample period equals ≈ 3 m.

In order to reduce this error, two alternative configurations were tested:

10 MHz synchronization

The reference input of the sampler is connected to the AMIQs reference output. The error is the same as for the unsynchronized configuration, but the frequency difference between the two sample clocks seems to be constant. The reason for that is AMIQ's clock synthesizer that can't generate exactly 47.5 or 95 MHz.

Synchronization of the sample clocks

The receiver locks his sample clock to the AMIQs sample clock, where the common sample rate is 95 MHz. In this configuration, the synchronization works quite fine, the mean error is reduced to ≈ 1 mm. Figure 5.9 (b) shows the estimated signal position for the first eight hours after power on. After about three hours of operation the drift of the position is ≈ -1 mm/h.

In this configuration, the attenuation due to the sinc distortion described in Section 5.1.1 is ≈ 0.7 dB at 21 MHz, so that the the pre equalization filter in the transmitter may be omitted.

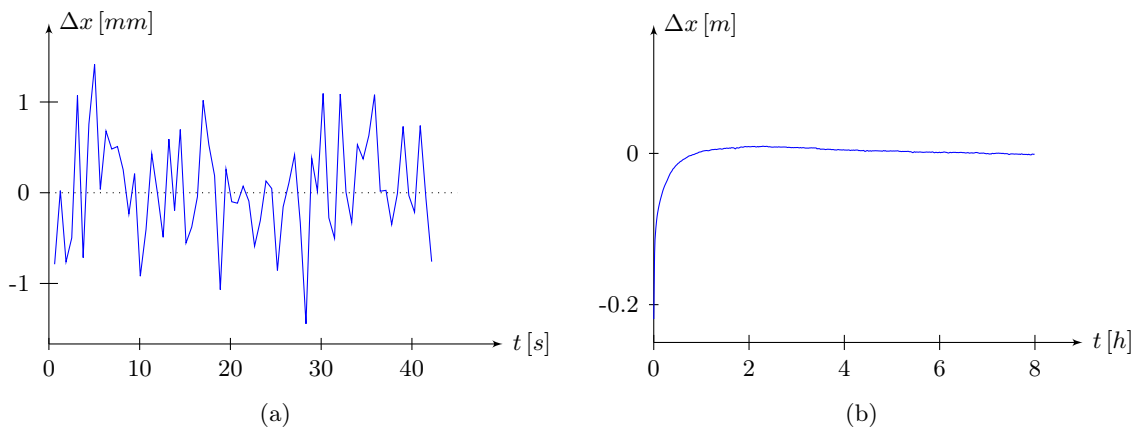


Figure 5.9: Synchronization of the sample clocks: The estimated signal delays (a) after three hours of operation and (b) for the first eight hours after power on.

Even though the synchronization of the sample clocks works quite fine:

All measurements of distances and distance differences are based on a known receiver sample frequency. In order to make exact measurements, the exact sample frequency has to be known.

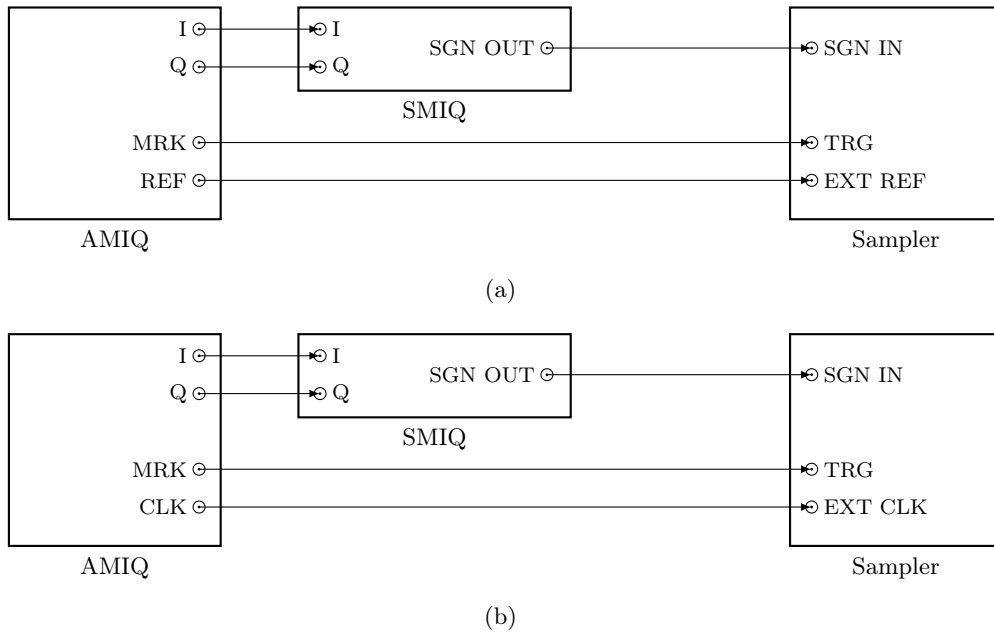


Figure 5.10: Configurations for synchronization (a) using the 10 MHz reference (b) using the transmitters sample clock.

Chapter 6

Measurements

In this chapter, the measurements recorded with the measurement setup from Chapter 5 are presented.

The influence of the receiver noise is investigated and compared to the results of the calculation. The receiver noise is also used to show the function and the limits of the zero forcing equalizer used in the receiver.

6.1 Aspects

In order to make useful measurements, a few aspects should be considered:

- In the used configuration of the system where both, the transmitter and the receiver use a sample clock of 95 MHz, two different sample clocks have to be used in MATLAB. While the transmit signal is calculated for the transmitters sample frequency of 95 MHz, the received signal is decimated to 47.5 MHz before it is transmitted to MATLAB.
- For all measurements a sample frequency of exact 95 MHz is assumed.
- The time difference between the arrival of the trigger and the next sample pulse is approximately constant, but remains unknown. Measuring distances can only be done based upon the difference to a reference distance.
- When using other chiprates than 47.5 MHz, the length of one signal period should always be an integer value of samples. For the sake of simplicity the sample rate should be an integer multiple of the chiprate.
- The phase of the received signal varies from measurement to measurement. Since it doesn't matter if the real value of the phase corrected correlation function or the magnitude of the complex correlation function is maximized, no phase estimation and correction has to be done. However, in case data is transmitted, the decoding needs a correct phase.
- The receiver noise is converted to the baseband the same way as the received signal, so it is complex as well. In investigations about the influence of the receiver noise, only half of the power of the complex noise has to be taken in account for real valued baseband signals.
- In the passband to baseband transformation performed in the sampler, where the negative frequency components of the transmit signal are discarded and the positive components are shifted to the baseband, the power of the baseband signal equals the power of the positive components. To obtain the received (passband) power, the power of the baseband signal has to be multiplied by a factor of two.
- In order to calculate the correct receive power, the input equalizer has to be normalized.

6.2 White gaussian noise

The noise at the receiver input is now assumed to be white and gaussian thermal noise. The mean positioning error caused by this noise is measured and compared to the results of the calculation in Chapter 3.

The mean error as a function of the SNR

In this measurement, the standard deviation of the position estimation was determined for different values of the transmit power. The signal position was measured 500 times for every value of the transmit power. The SNR was then calculated by dividing the transmit power by the received power of the equalized input signal when the transmit signal was turned off. As mentioned in Section 6.1, only half of the power of the complex valued receiver noise influences the transmission.

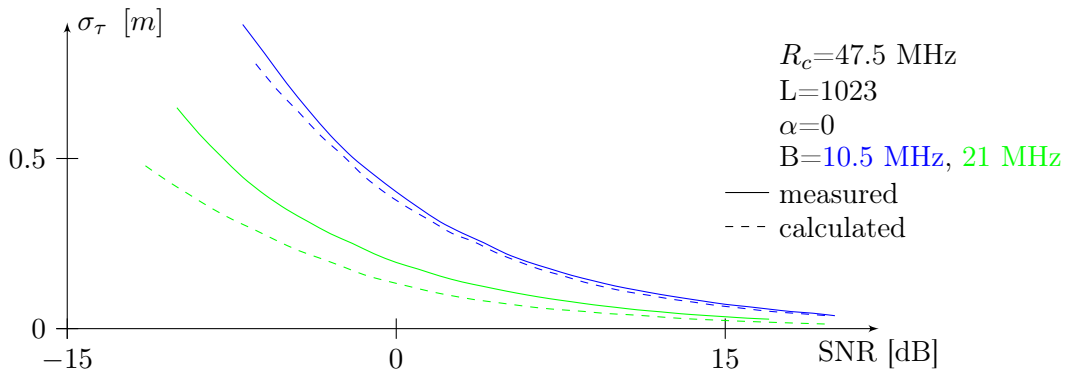


Figure 6.1: Mean error as a function of the SNR: The higher the bandwidth, the higher the difference between the measurement and the calculation.

Figure 6.1 shows the results for sinc pulses with different bandwidths. While the measured and the simulated curves are nearly identical for a bandwidth of 10.5 MHz, the difference for a bandwidth of 21 MHz (\approx the -3 dB bandwidth of the sampler) is ≈ 3 dB (the calculated curve is shifted to the right by 3 dB). Without the equalizer, the difference to the calculation is much higher.

The mean error as a function of the signal bandwidth

Following the Cramer Rao lower bound for the standard deviation derived in Section 3.3, the standard deviation depends on the signal-to-noise ratio in the same way, independent of any other signal parameter. Thus it is not necessary to measure the standard deviation for more than one value of the received power to see the difference between the calculation and the measurement. This fact was used to evaluate the influence of the input filters and the equalizer.

In the measurement, a constant signal-to-noise ratio (as ratio of the signal power to the noise PSD) was used. This was achieved by using a constant signal power of -43 dBm, and a constant sampler input range of 10 dBm for all signals. To compare the measurement with the calculation, the noise power at 10 MHz was measured and divided by 10 MHz, resulting in a signal-to-noise ratio $\frac{C}{N_0}$ of 82 dB-Hz.

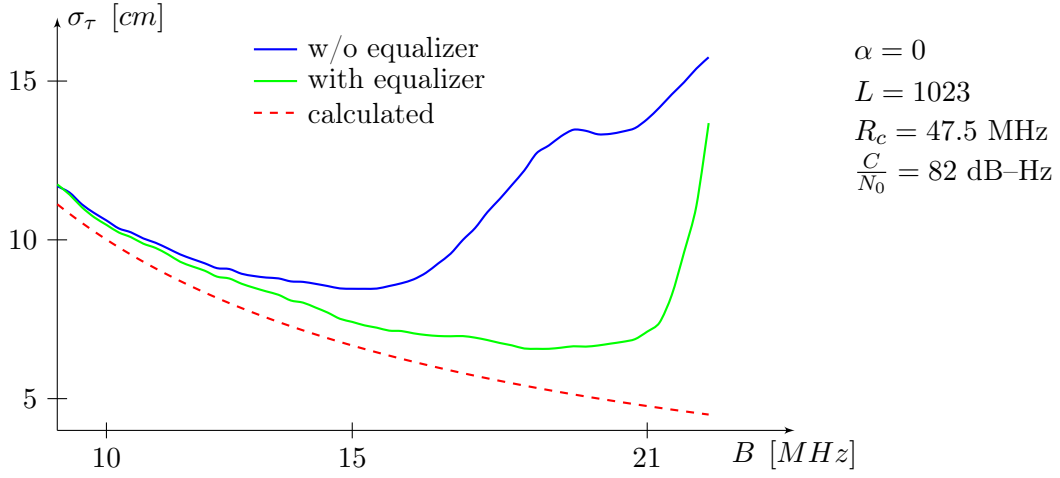


Figure 6.2: Influence of the equalizer for $\alpha = 0$

Figure 6.2 shows the results for sinc pulses. For signal bandwidths higher than ≈ 11 MHz, the influence of the equalizer becomes evident. While the mean error should decrease for an increasing bandwidth, the mean error of the unequalized signal is increasing. The mean error of the equalized signal is quite close to the calculation for bandwidths up to ≈ 21 MHz, while for bandwidths above, the noise amplification due to the zero forcing equalizer becomes evident. At a bandwidth of 21 MHz, the error of the unequalized signal is ≈ 6 dB higher than for the equalized signal. This break may be used to define 21 MHz as the maximum useful bandwidth for sinc pulses.

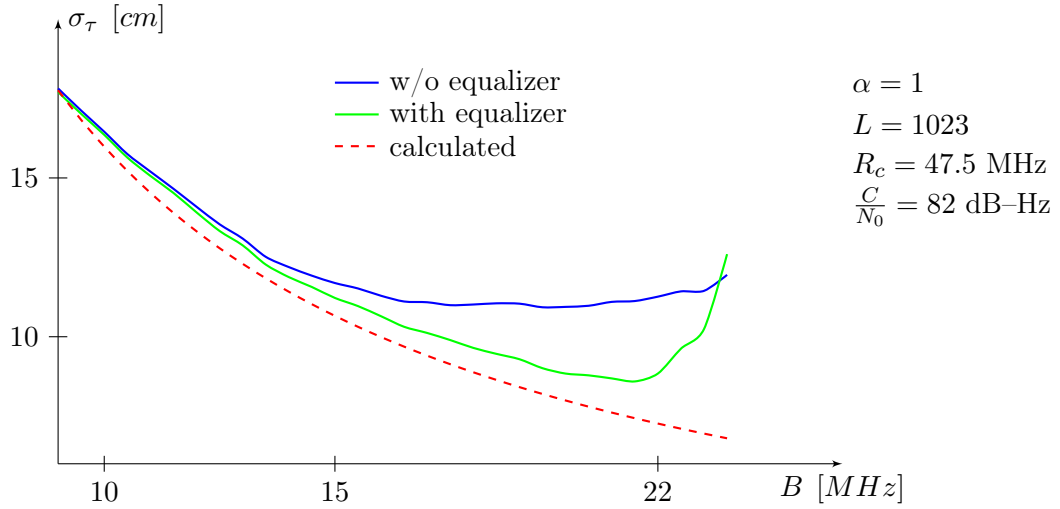


Figure 6.3: Influence of the equalizer for $\alpha = 1$

Now a root raised cosine pulse with $\alpha = 1$ which has less high frequency components than the sinc pulse is used. In contrast to the sinc pulse, the difference between the equalized and the unequalized signals is not that high. The maximum bandwidth is ≈ 22 MHz, 1 MHz higher as for sinc pulses.

Chapter 7

Conclusion

Positioning and ranging systems, working with the propagation delay from different sources in order to derive the current position, often make use of direct spread spectrum modulation techniques. This work covered four major topics. First, the basics of the transmission signal and direct sequence spread spectrum modulation were explained. Secondly, the influence of white gaussian noise was analyzed by simulations and analytical calculations. Thirdly, the impact of multipath propagation onto the ranging accuracy of the system was studied using a MATLAB simulation setup. Finally, a hardware testbed for the purpose of measuring the influence of noise and multipath propagation was set up. The following paragraphs describe the four steps and the corresponding results in greater detail.

Direct sequence spread spectrum modulation

Direct sequence spread spectrum is a proper modulation technique for positioning and ranging applications. The influence of noise and multipath propagation is the smaller the higher the transmit bandwidth. Due to the CDMA capability of direct sequence spread spectrum modulation, different transmitters can share the same channel, each with the maximum available bandwidth.

Using the matched filter approach to spread spectrum, simulations and measurements can be done by transmitting and processing just a single period of the transmit signal. All signal processing may then be done in the frequency domain using the FFT.

White gaussian noise

The influence of white gaussian noise on the estimation of the propagation time of a signal can be simulated as well as derived using the Cramer Rao lower bound. For a given signal-to-noise ratio, the accuracy is the higher, the higher the bandwidth of the transmit signal. For a given bandwidth, root raised cosine pulses are more accurate than bandlimited rectangular pulses, while the accuracy is the higher, the lower the roll-off factor of the root raised cosine pulses. Another parameter the accuracy depends on is the observation time. This parameter is usually set in the transmitter by defining a certain symbol duration. In order to achieve a higher accuracy, the observation time may be increased in the receiver.

Multipath propagation

The influence of multipath propagation was simulated for a very simple channel model, whereas other, more complex models may also be simulated using the MATLAB simulation system. For the simple model, the error caused by multipath propagation depends only on the shape of the used pulse. The error is the higher, the lower the bandwidth of the pulse. For rectangular and root raised cosine pulses with high roll-off factor, significant errors only occur for distance

differences between different paths smaller than a certain bound. The lower the roll-off factor of root raised cosine pulses, the higher this bound. However, the minimum error is obtained for sinc pulses.

Measurements

A measurement system that is capable of measuring the time of arrival of a signal relative to the arrival of a trigger with an equivalent accuracy of approximately 1 mm was set up and tested. It may be used for signals with a bandwidth of up to 21 MHz. The influence of the receiver noise was measured and compared to the result of the calculation for white gaussian noise, whereas the results of the measurement come very close to the calculation.

Bibliography

- [1] Alois M. J. Goiser. *Handbuch der Spread-Spectrum Technik*. Springer Verlag, 1998.
- [2] Franz Hlawatsch. Analog and digital communication techniques. Technical report, TU Vienna, Institute of Communications and Radio-Frequency Engineering, 2003.
- [3] Lawrence R. Weill, Nobuhiro Kishimoto, Seiichiro Hirata, and Kevin Xinhua Chin. The next generation of a super sensitive gps system. In *Proceedings of the 17th International Technical Meeting of the Satellite Division of the Institute of Navigation ION GNSS 2004*, pages 1924–1935, 2004.
- [4] Mohinder S. Grewal, Lawrence R. Weill, and Angus P. Andrews. *Global Positioning Systems, Inertial Navigation and Integration*. John Wiley & Sons, 2001.
- [5] Rohde & Schwarz. *I/Q Modulation Generator AMIQ*.
- [6] Maxim Integrated Products. *Equalizing Techniques Flatten DAC Frequency Response*, 2005.
- [7] Rohde & Schwarz. *Vector Signal Generator SMIQ*.
- [8] Agilent Technologies. *E1439 VXI 70 MHz IF ADC Users's Guide*.

Appendix A

The Demonstration GUI

For the purpose of demonstrating the function of the measurement system, I programmed a graphical user interface in MATLAB.

The major features of the GUI are:

- The signal parameters, such as the bandwidth and the roll-off factor are set before starting the GUI.
- The received signal is continuously sampled in blocks of one signal period and is sent to the GUI where the signal is processed.
- An equalizer is automatically calculated and applied to the received signal. It can be recalculated and switched on and off during operation.
- The received power is calculated and displayed.
- The estimated position of the maximum is saved in an array, whereas the mean value and the standard deviation of the last N (an arbitrary number that can be set at startup) estimated positions is displayed.
- The GUI's upper figure (see Figure A.1 to A.4) shows the correlation function at the output of the demodulator. The *zoom button* switches between the display of the entire period and the range around the correlation maximum.
- The lower figure can display three different types of plots:
 - **Spectr:** shows the power spectrum of the received signal.
 - **Hist:** shows a histogram of the saved positions.
 - **Pos:** shows the saved signal positions.
- Optionally, data that was defined at startup and is periodically transmitted can be demodulated by the GUI. The received data is demodulated and displayed as ASCII coded string. The phase is estimated using the first symbol, that is always "1".

Figure A.1 shows the GUI for a quite strong signal, where a cable¹ having a length of approximately 6 m was inserted into the signal path. The lower figure shows the estimated signal positions, whereas the standard deviation is approximately 3 mm. In Figure A.2, the demodulation of data is illustrated. Figure A.3 shows the distortion caused by a short circuited cable that was connected in parallel to the signal path. The last picture shows the histogram of the estimated position for a signal-to-noise ratio of approximately 0 dB.

¹A propagation speed of $0.66 \cdot c_0$ was assumed.

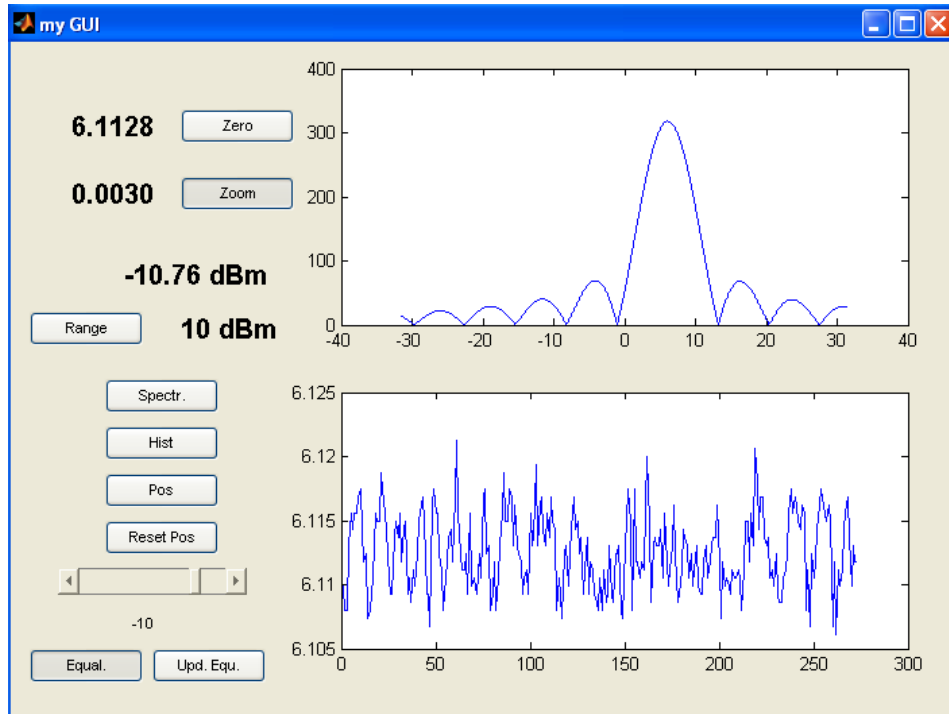


Figure A.1: Demonstration GUI.

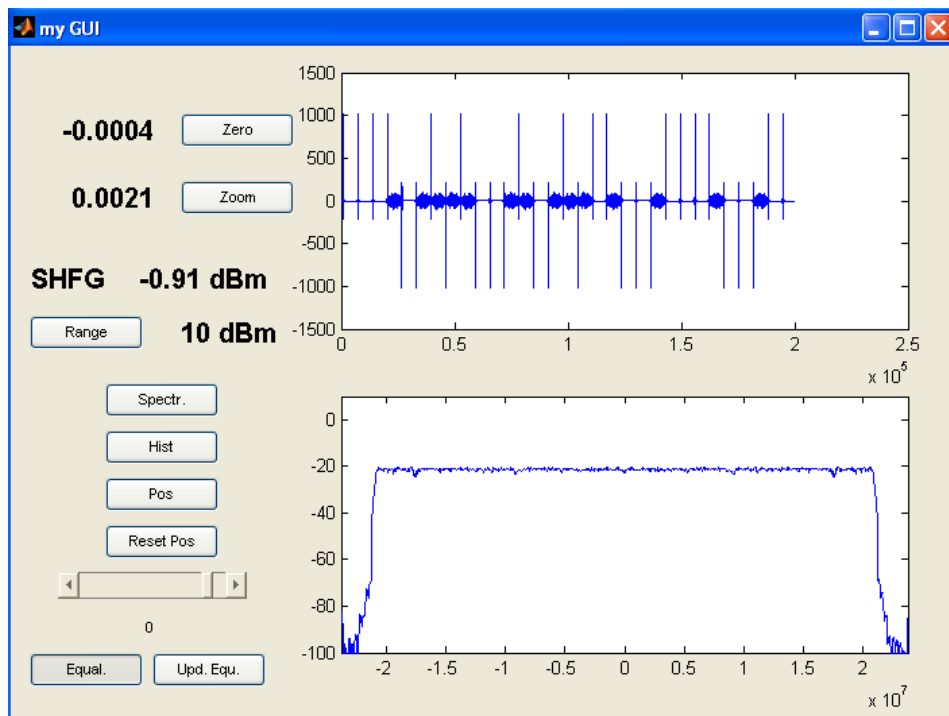


Figure A.2: Demodulated data: The ascii representation of the string "SHFG" is transmitted, demodulated and displayed.

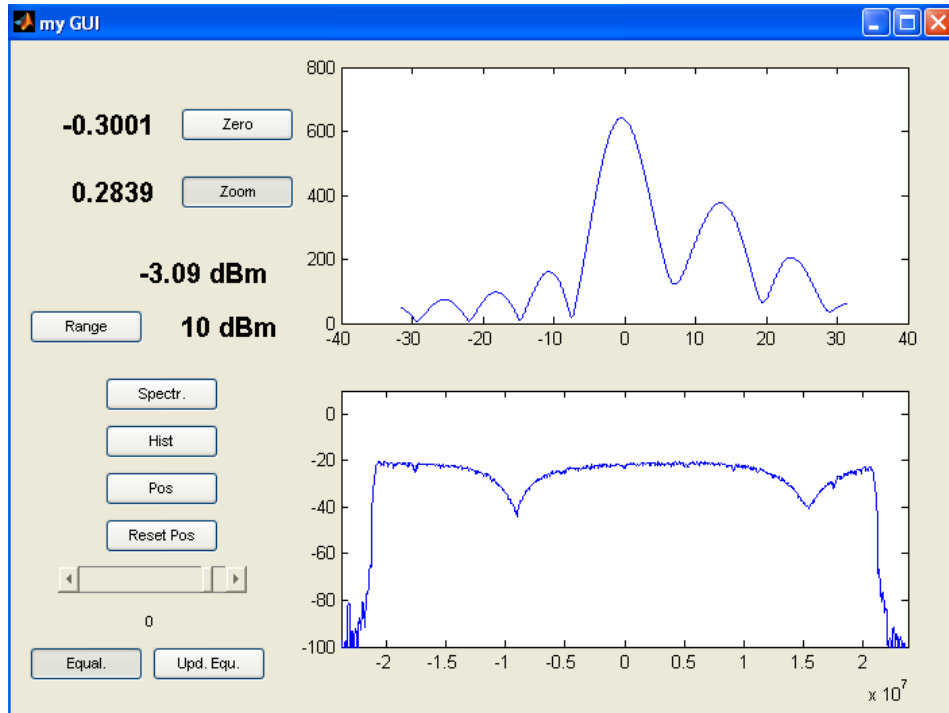


Figure A.3: Channel distortion in the time and frequency domain.

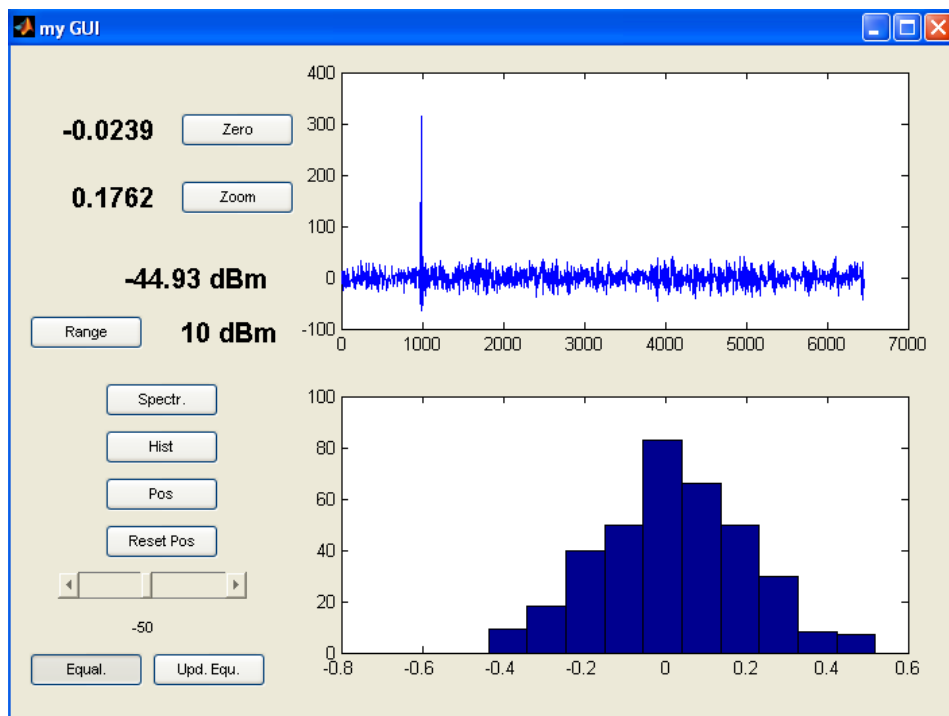


Figure A.4: Histogram of the estimated signal positions for a SNR of ≈ 0 dB.